Diagnosis, maintenance, retrofitting, repair

Stud Arrangement to Reduce Fatigue Cracks and Application of Drilled Holes

Ichiro OKURA
Associate Professor
Osaka University
Suita, Osaka 565, Japan

Born in 1955, Ichiro Okura attended Osaka University, earning his doctorate in civil engineering in 1985. His research focuses on fatigue and fracture in steel bridges.

Summary

This paper presents the arrangement of stud shear connectors to reduce the fatigue cracks at the connections of cross beams to main girders and at the top of intermediate vertical stiffeners in highway bridges. Fatigue tests are carried out on the specimens consisting of a concrete slab and two main girders. Finite element models for the transfer of load between a concrete slab and a top flange of a main girder are developed. Drilled holes are shown to be effective to stop the propagation of the cracks in main girder webs.

1. Introduction

In many plate girder highway bridges in the urban areas of Japan, such fatigue cracks as shown in Fig.1 are detected at the connections of cross beams to main girders [1]. In some bridges, they are also observed at the top of intermediate vertical stiffeners to which cross beams are not connected. This paper presents the arrangement of stud shear connectors to reduce those cracks. Fatigue tests are carried out on the specimens consisting of a concrete slab and two main girders. Finite element models for the transfer of load between a concrete slab and a top flange of a main girder are developed. Drilled holes are shown to be effective to stop the propagation of the cracks in main girder webs.

2. Fatigue Tests

The specimens of the fatigue tests are shown in Fig.2 [2]. A cross beam is provided in the specimens B, while it is not in the specimens A. The interval between the main girders is 2 m. The concrete slab 16 cm thick and 168 cm wide in the bridge-axis direction is made from lightweight-aggregate concrete. Two pieces were prepared for each of the specimens A and B. Fig.3 shows the stud arrangement on the main girders of the specimens. Studs are put just on the vertical stiffener of the main girder A1-G1 and on the connection plate of the main girder B1-G1.

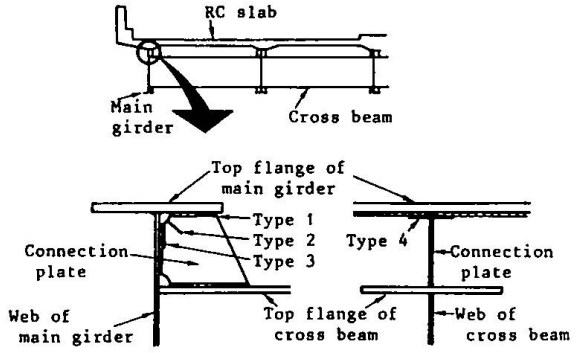

Fig.1 Fatigue cracks at cross-beam connections

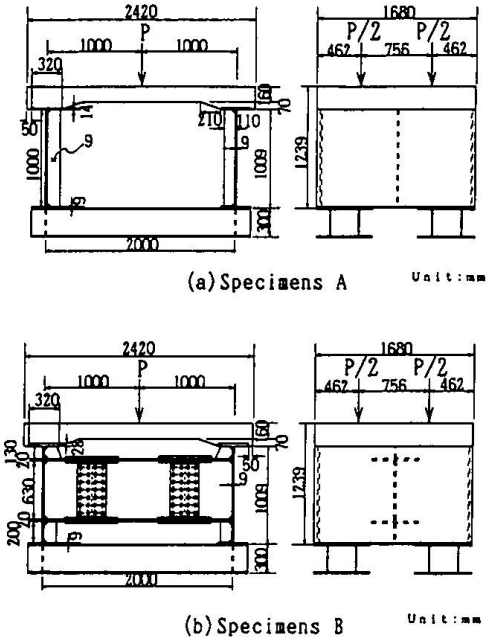

Fig.2 Fatigue test specimens

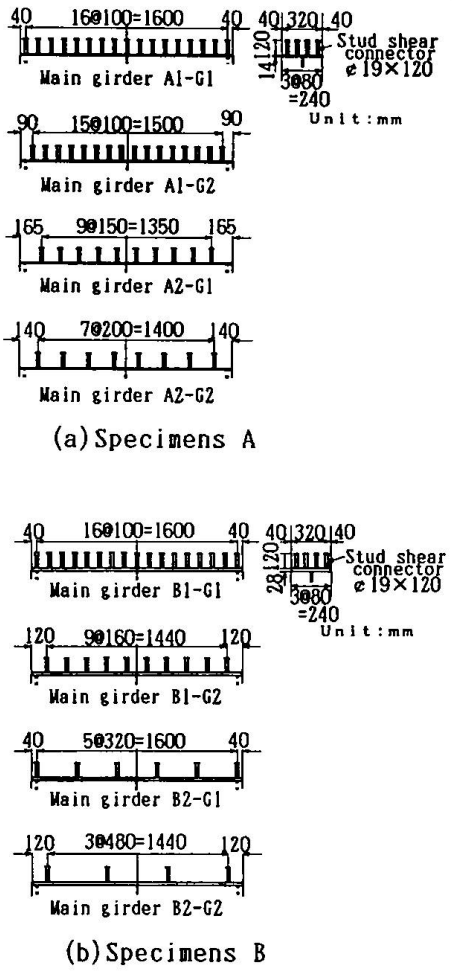

Fig.3 Stud arrangement

In other main girders, studs are not located on the connection plate or the vertical stiffener. The studs used are 19 mm in diameter and 120 mm in height.

Static loading tests were conducted before fatigue tests. To examine the relations between the slab deformation and the local stresses influential for the cracks, equal loads were applied downward at two points 75.6 cm apart in the bridge-axis direction on the top surface of the slab, in the middle between the main girders. Next, the loads were applied upward at the same locations on the bottom surface of the slab. As schematically shown in Fig.4(a), for a load between the main girders G_1 and G_2 in an actual bridge, the slab is deformed in a downward convex form between the main girders G_1 and G_2 and in an upward convex form between the main girders G_2 and G_3. In the static loading tests, the downward and upward convex forms of the slab deformation are given by such loading conditions as shown in Figs.4(b) and (c), respectively. Here, the slab deformations in Figs.4(b) and (c) are named slab-positive deformation and slab-negative deformation, respectively.

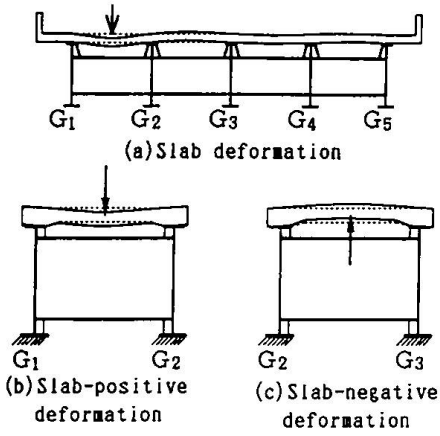

Fig.4 Positive and negative deformations of slab

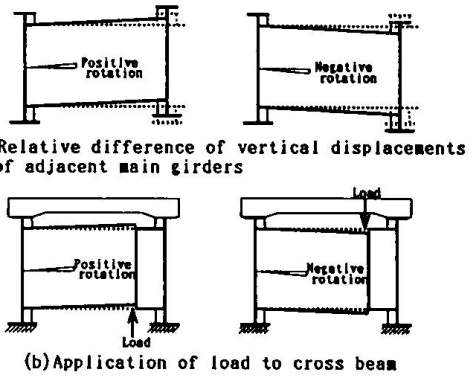

Fig.5 Positive and negative rotations of cross beam

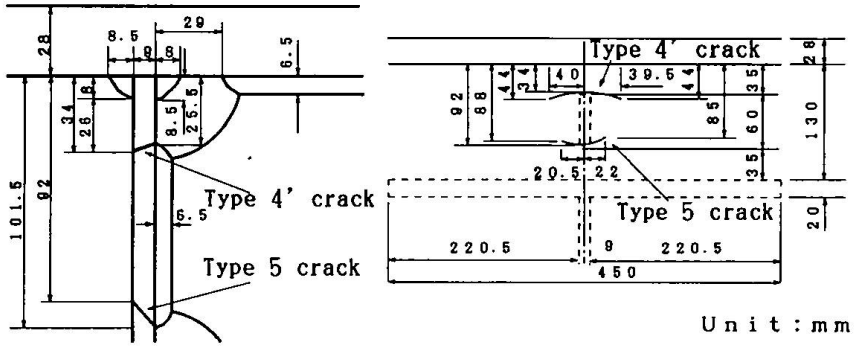

Fig.6 Types 4' and 5 fatigue cracks at 5.1×10^6 cycles [Main girder B2-G1]

To investigate the relations between the cross-beam rotation and the local stresses, the bolted connection at one end of the cross beam in the specimens B was loosened, and an upward or downward load was applied to this end. As shown in Fig.5(a), positive and negative rotations are produced at the end of a cross beam in an actual bridge, depending on the relative difference of the vertical displacements of adjacent main girders. In the static loading tests, as shown in Fig.5(b), the application of a vertical load to one end of the cross beam induces positive and negative rotations at the other end.

The fatigue tests were accomplished on the specimens A1, B1 and B2 under the slab-positive deformation shown in Fig.4(b) at ΔP = 93.1 kN and 142.1 kN. Type 1 crack such as shown in Fig.1 was initiated in the connection plate or at the top of the vertical stiffener of each main girder of the three specimens. However, the crack grew very slowly, and stopped after the propagation of about 10 mm. As shown in Fig.6, the specimen B1 suffered Type 4' crack in the web of each main girder, and the specimen B2 experienced Type 4' and 5 cracks. Types 4' and 5 cracks were initiated at the toes on the web side of the upper and lower end returns of the fillet weld between the connection plate and the main girder web, respectively. Both cracks penetrated the web, and propagated horizontally in the web.

In the specimen B1, drilled holes 25 mm in diameter were provided at the tips of Type 4' crack at 10 million cycles of loading [Case(I)]. The hole edge was smoothed by sandpaper. No cracks

were created at the drilled holes during 2 million cycles after the resumption of the test. In actual bridges, there are instances that connection plates are separated from the top flange and/or the web of main girders due to the propagation of Types 1, 2 and 3 cracks. Then, the connection plate was flame-cut along the fillet weld between the connection plate and the top flange of the main girder [Case(II)]. The test continued by 2 million cycles without cracks at the drilled holes. Moreover the connection plate was flame-cut along the fillet weld between the connection plate and the main girder web [Case(III)]. The test carried on by 2 million cycles with the result of no cracking at the drilled holes.

3. Finite Element Models for Test Specimens

In the static loading tests, it was observed that as shown in Fig.7, the slab rotated at the edges A and B on the top flange of the main girder for the slab-positive and -negative deformations, respectively. Likewise, as shown in Fig.8, the top flange rotated at its edges A and B for the cross-beam-positive and -negative rotations, respectively. Fig.9 shows finite element models for the transfer of load between a concrete slab and a top flange of a main girder through those observations. Fig.9(a) corresponds to the slab-positive deformation and the cross-beam-positive rotation. Fig.9(b) corresponds to the slab-negative deformation and the cross-beam-negative rotation. In the finite element analysis, rectangular and triangular plate elements with 6 degrees of freedom at each node are used [3]. In Fig.9(a) rigid beams with hinges at both ends connect the nodes on the edge A-A on the neutral plane of the top flange to those on the neutral plane of the slab, and in Fig.9(b) they do so on the edge B-B. For the studs, beam elements with the stiffness of the studs join both nodes on the neutral planes of the top flange and the slab.

As an example, Fig.10 presents the mesh division for the specimen B1 with loads applied to the slab and drilled holes provided at the tips of Type 4' cracks. Type 4' crack and the flame cutting of the connection plate are expressed by double nodes. As shown in Fig.3, the stud arrangement is different on the right and left main girders of the specimens. Due to the limitations of calculation capacity of the computer, the quarter of the specimen is divided into finite elements. The boundary condition of symmetry was imposed on the cut sections. The bottoms of the web and the vertical stiffener of the main girder were fixed.

4. Stud Arrangement to Reduce Fatigue Cracks

The finite element analysis was carried out for the stud spacing which was not considered in the fatigue tests [4]. Combining the relations between the stud spacing and the local stresses which are obtained from the finite element analysis and the previous researches [5-7] gives us the following conclusion on the arrangement of studs to reduce the fatigue cracks:

Keeping studs away from the locations of connection plates and vertical stiffeners has an effect on the reduction of the fatigue cracks for interior main girders. However, it does not for exterior main girders.

Usually, the stud spacing is determined by the shear force in the bridge-axis direction between a top flange of a steel girder and a concrete slab. In order to reduce the fatigue cracks in interior main girders, studs should be placed as far as possible from the locations of connection plates and vertical stiffeners, not exceeding the stud spacing determined by the shear force.

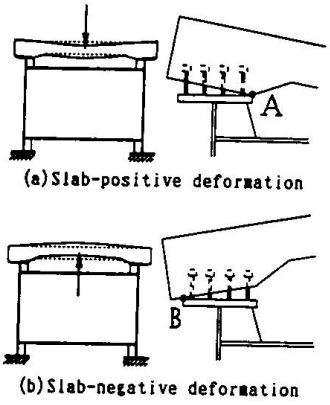

Fig.7 Behavior between slab and flange for slab deformation

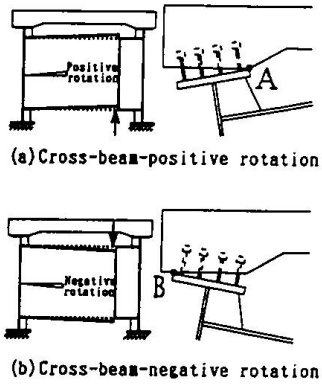

Fig.8 Behavior between slab and flange for cross-beam rotation

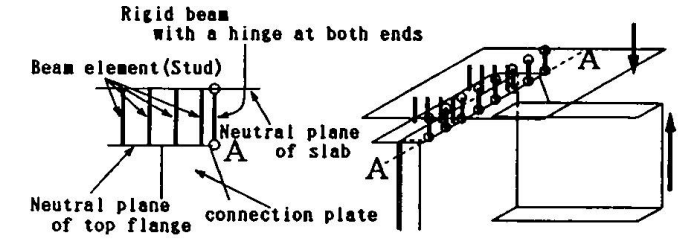

(a) Load-transfer-model for slab-positive deformation and cross-beam-positive rotation

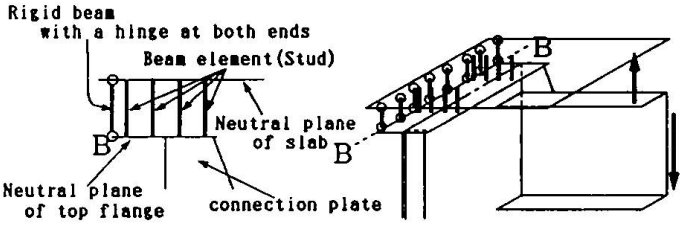

(b) Load-transfer-model for slab-negative deformation and cross-beam-negative rotation

Fig.9 Load-transfer-model between slab and flange

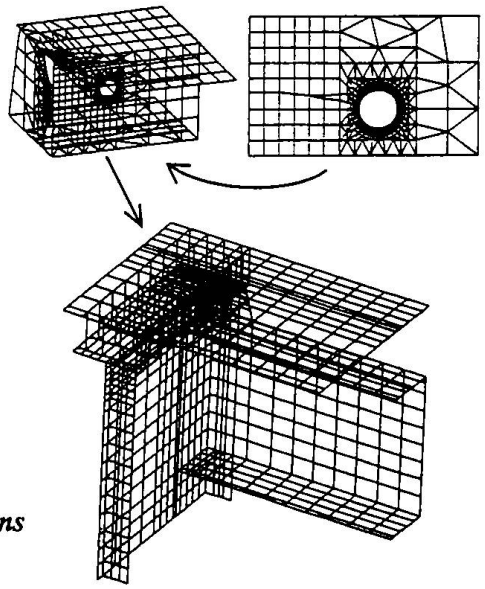

Fig.10 Mesh division for specimens

5. Effectiveness of Drilled Holes

The condition to prevent drilled holes from cracking is as follows [8]:

$$\Delta\sigma_f < 213\sqrt{\sigma_Y} \quad (1)$$

where $\Delta\sigma_f$ = stress range at the edge of drilled holes (in MPa), and σ_Y = yielding stress of steel

plates in which the drilled holes are provided (in MPa).
The stress range $\Delta\sigma_t$ at the drilled hole edge is estimated by the following equation [8]:

$$\Delta\sigma_t = 1.05\Delta\sigma_{m(FEM)} + \frac{1.766 + 3.464\,\rho/t}{1 + 3.539\,\rho/t}\Delta\sigma_{b(FEM)} \quad (2)$$

where $\Delta\sigma_{m(FEM)}$ and $\Delta\sigma_{b(FEM)}$ = membrane and plate-bending stresses at the drilled hole edge computed by the finite element analysis with plate elements, respectively, ρ = radius of drilled holes, and t = thickness of steel plates.

Since ρ and t of the specimen are 12.5 mm and 9 mm, respectively, its stress range $\Delta\sigma_t$ is calculated by

$$\Delta\sigma_t = 1.05\Delta\sigma_{m(FEM)} + 1.11\Delta\sigma_{b(FEM)} \quad (3)$$

The membrane and plate-bending stresses in the tangential direction at the drilled hole edge are used for $\Delta\sigma_{m(FEM)}$ and $\Delta\sigma_{b(FEM)}$, respectively. The maximum of $\Delta\sigma_t$ is 112.7 MPa in the cases (I), (II) and (III), which are defined in the fatigue tests. This value is much smaller than $213\sqrt{\sigma_Y} = 450.6$ MPa in Eq.(1), where the yielding stress σ_Y of the specimen is 447.6 MPa. This explains why there was no crack initiation at the drilled holes in the specimen.

6. Conclusion

The arrangement of stud shear connectors to reduce the fatigue cracks at connection plates and vertical stiffeners was presented. Drilled holes were shown to be effective to stop the propagation of the cracks in main girder webs.

References

[1] OKURA, I. *Fatigue in Steel Bridges.* (in Japanese) Toyo-shoten Publisher, Tokyo, Japan, 1994.
[2] OKURA, I.; SAKAMOTO, H.; SHIOZAKI, T.; FUKUMOTO, Y. *Local stresses and fatigue cracks at the top of vertical stiffeners of plate girders.* (in Japanese) J. Structural Eng., JSCE, Japan, Vol.40A, 1994, pp.1087-1100.
[3] ISAP (Integrated Analysis Program), NEC Corporation, FXI 52-10, Tokyo, Japan, 1989.
[4] OKURA, I.; SHIOZAKI, T.; FUKUMOTO, Y.; NANJYO, A. *Stud arrangement to reduce fatigue cracking in vertical stiffeners.* J. Structural Eng./Earthquake Eng., JSCE, Japan, Vol.13, No.1, 1996, pp.55s-66s.
[5] OKURA, I.; FUKUMOTO, Y. *Fatigue of cross beam connections in steel bridges.* Proc., IABSE 13th Congress, Helsinki, Finland, 1988, pp.741-746.
[6] OKURA, I.; FUKUMOTO, Y. *Fatigue of cross-beam connections in plate girder highway bridges.* Proc., IABSE Workshop, Lausanne, Switzerland, 1990, pp.167-176.
[7] OKURA, I.; FUKUMOTO, Y. *Fatigue tests of cross-beam connections in plate girder highway bridges.* Porc., First World Conference on Constructional Steel Design, Acapulco, Mexico, 1992, pp.466-469.
[8] OKURA, I.; SHIOZAKI, T.; NAKANISHI, Y. *Fatigue strength of drilled holes under membrane and plate-bending stresses.* (in Japanese) J. Structural Eng./Earthquake Eng., JSCE, Japan, No.537/I-35, 1996, pp.327-338.

The Performance of Coiled Spring Pin Connectors under Static and Fatigue Loading

Roger BUCKBY
Director
Sir William Halcrow & Partners Ltd
Swindon, England

Martin OGLE
Principal Design
TWI, Abington Hall
Cambridge, England

Roger Paul JOHNSON
Professor of Civil Eng.
University of Warwick
Coventry, England

David HARVEY
Manager
Associated Engineering (BC) Ltd
Vancouver, BC, Canada

Summary

Coiled spring pin connectors provide a simple low-cost method for upgrading the fatigue life of composite bridges, but their satisfactory performance is dependent on achieving a close tolerance fit between the pins and the steel and concrete elements into which they are installed. The authors describe the behaviour of coiled spring pin connectors observed in fifteen shear (push-out) tests under static and constant amplitude repeated loading. The tests were commissioned to validate the retrofit design and installation of this type of connector for upgrading the fatigue life of a multi-span composite box girder structure carrying a mass rapid transit system in Canada. The retrofit installation was completed in 1995.

1. Introduction

Coiled spring pins are widely used as fasteners in the mechanical engineering industry, but have found relatively little application on civil engineering projects. They were first used to upgrade the fatigue life of composite plate girder bridges on the Docklands Light Railway, London in 1988. The test data available from that application were considered to be insufficient to validate their use on the Canadian project to which the authors refer and a series of static and fatigue tests was commissioned at TWI, Cambridge to obtain further data on the load-slip behaviour under static and constant-amplitude shear loading.

2. Test Specimens

Fifteen specimens with a reinforced concrete block cast between two parallel steel plates were fabricated to the dimensions shown in Figure 1. The density of reinforcement in the block was based upon the requirements of BS5400 Part 5. Steel straps were welded to the side plates to resist the forces of separation. In the structure, these forces are resisted by the heads of the existing welded stud connectors. Plate thicknesses of 25mm and 35mm, which were representative of the majority of flange plates in the structure were used to study the influence of plate thickness on load-slip behaviour. Four 175mm long x 20mm dia heavy duty zinc plated pins were installed in each specimen. The pins were manufactured by Spirol Industries Limited to IS08748.The diameters of the pins and of the holes into which the pins were installed were carefully measured to ensure the test specimens were representative of the tolerances specified for the retrofit scheme. In two specimens, the pins were lightly coated with molybdenium disulphide grease before insertion to reproduce conditions on a small number of pins in the actual structure where grease was used to reduce the jacking load.

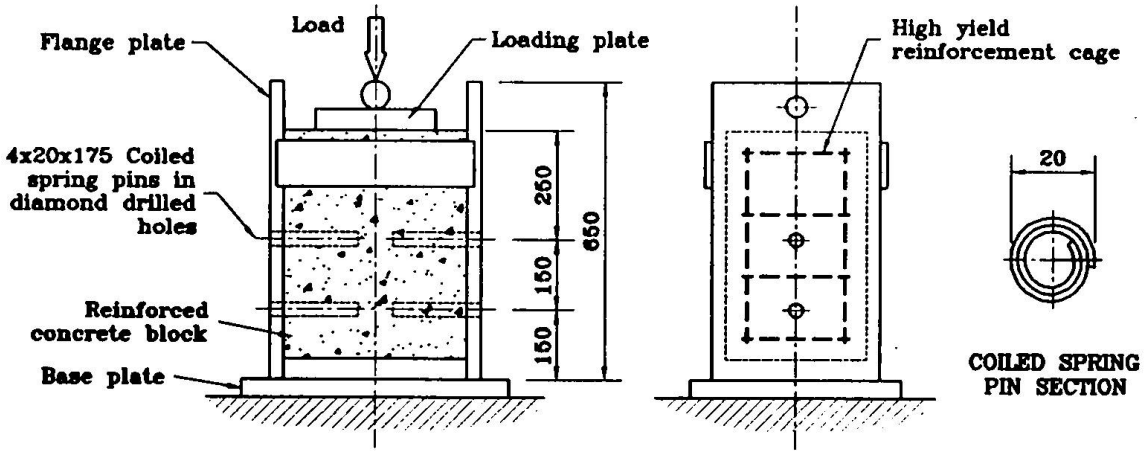

Figure 1 Test Specimens

3. Load Testing

Three specimens were loaded through their central axis to failure at a constant static loading rate of 1mm/min. The remaining 12 specimens were subjected to constant amplitude cyclic loading at a uniform frequency of either 8.3 or 10 Hz. Prior to fatigue testing, each specimen was subjected to three shakedown cycles. The purpose of the shakedown tests was to ensure that any residual bond between the concrete slab and steel plate was broken before the start of the fatigue loading test, but useful information was also obtained on the shear stiffness and the non-recoverable slip of the pins on initial loading and on subsequent unloading/reloading over three static loading cycles.

4. Load-Slip Behaviour under Static Shear Loading

The load-slip behaviour of one of the three specimens subjected to static loading is shown in Figure 2. The similarity of the results for all these specimens was remarkably consistent. Slip measurements on the specimens were terminated at 20mm, but even at slips up to 38mm, the pins continued to carry more than 70 per cent of their ultimate load, due to progressive cracking at different locations in the pins and shear cracking of the concrete block due to yielding of the transverse reinforcement.

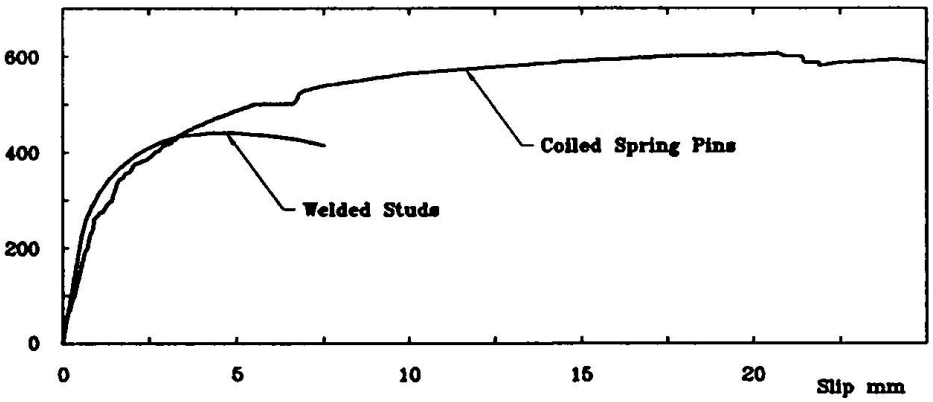

Figure 2 Typical Load-Slip Behaviour of Specimen Under Static Shear Loading

From these three tests, the static nominal ultimate load of a 20mm diameter pin, P_u, was determined as 130kN using the method recommended in Clause 5.3.2.4 of BS5400 Part 5 for tests on non-standard connectors. Figure 2 also shows the typical load-slip behaviour for a 100mm long x 19mm diameter welded stud embedded in concrete of similar strength for which

BS5400 Part 5 gives P_u = 107 kN. The effect of lightly greasing the pins in specimen 3 had a negligible effect on the ultimate load capacity but, as expected, slightly increased the slip for a given load.

5. Load-Slip Behaviour under Constant Amplitude Cyclic Loading

5.1 Shakedown Tests

The load-slip relationship observed in specimen 14 with a plate thickness of 35mm is shown in Figure 3 for the following conditions:

(i) on initial loading

(ii) on subsequent unloading/reloading over 3 cycles

(iii) on completion of 0.55 x 10^6 cycles of loading over the range 0.1 P_u - 0.44 P_u.

On the eight specimens tested with 35mm plates, the elastic stiffness of the pins on initial loading, K_{p1}, varied between 65 kN/mm to 110 kN/mm and after 3 cycles of loading, K_{p3}. between 65 - 120 kN/mm. In the specimens with 25mm plates, the stiffness of the pins on initial loading varied between 70-75 kN/mm and after 3 cycles of loading between 90 and 110 kN/mm.

On completion of the constant amplitude cyclic loading tests, the stiffness of the pins, K_{pf}, generally reduced, due to the formation of fatigue cracks in the specimen. However, on specimen 14, no significant loss of stiffness was observed on completion of the fatigue test at N = 0.55 x 10^6 cycles.

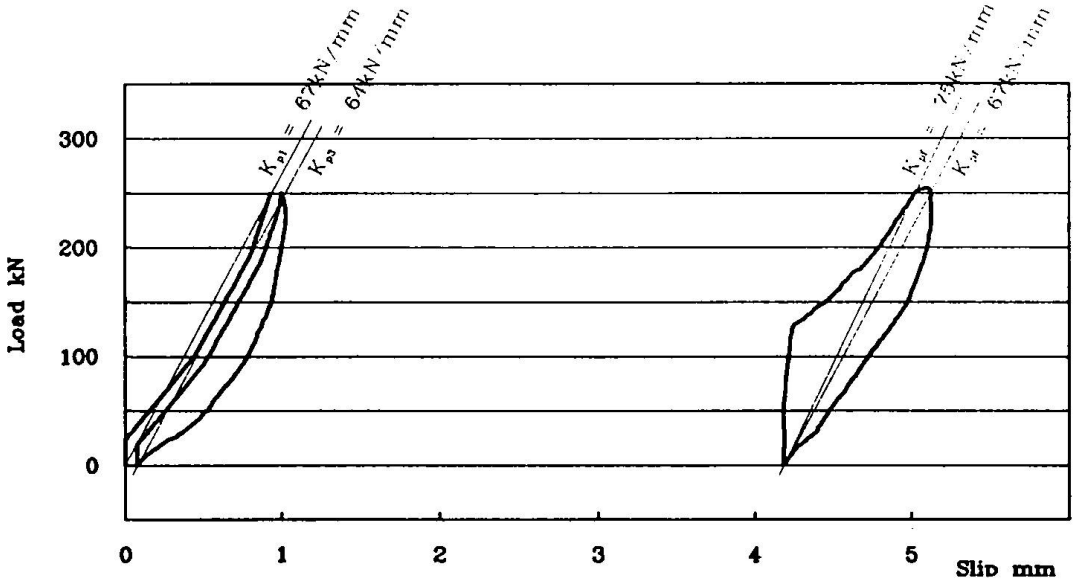

Figure 3 Typical Load-Slip Response in Specinien with 35mm Flanges

5.2 Load-Slip Behaviour under Constant Amplitude Cyclic Shear Loading

The shear displacement of the steel plate in relation to the concrete block under constant amplitude shear loading was logged against time on opposite faces of the test specimens. From these results, the mean slip for a given number of loading cycles was determined, as shown in Figure 4 for specimen 15.

The cyclic loading tests were generally terminated when the slip reached 5mm, but in five tests loaded in the range 0.1 P_u to 0.4 P_u, the specimens sustained more than 11 million cycles without exceeding 2.4mm slip displacement.

The cyclic shear loading tests demonstrated that fatigue failure of a coiled spring pin connector is quite different to that of a welded stud connector and cannot be defined in the same way as for a stud where failure is characterised by sudden failure of the entire shank of the stud with rapid loss of load at a clearly defined number of cycles of loading. Thus, for coiled spring pins, it was concluded that fatigue failure should be defined as the number of cycles of loading sustained for a given slip displacement.

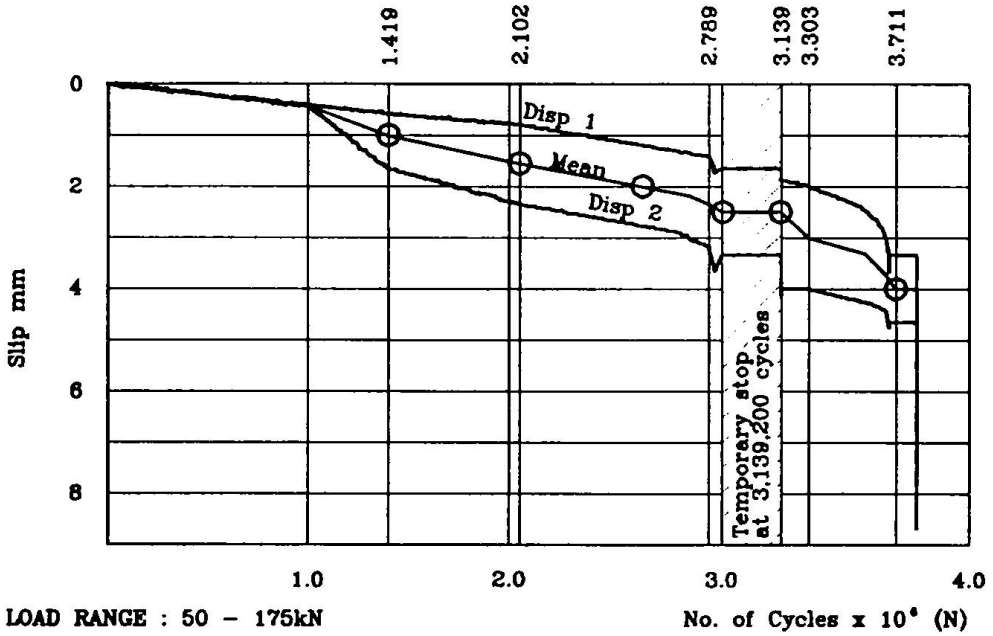

Figure 4 Typical Slip History for Specimen 15 with 35mm Flanges

In a retrofit scheme, if the new connectors are to share subsequently applied loadings more or less uniformly with the existing connectors, it is necessary that the connectors which are added are of a similar stiffness to the existing connectors.

For 19mm stud connectors, permanent slip under service loadings is generally in the range 1 to 2 mm so an upper limit of 2mm was adopted for Spirol pins.

The number of cycles of loading sustained by each specimen for different ranges of shear loading was then determined at slips of 1, 1.5mm and 2mm and was plotted as $\log_{10}P$ against $\log_{10}N$. The mean $\log_{10}P/\log_{10}N$ relationship of the test results was then obtained from a linear regression analysis of the test results and was compared with the mean value for 19mm stud connectors given in BS5400 Part 10.

In BS5400 Part 10, a probability of failure of 2.3% is adopted for the design of all welded details, including stud shear connectors. A low probability is appropriate for welded studs because fatigue failure of a stud is characterised by sudden loss of loading caused by fatigue failure of the weld at the root of the connector or in the shank itself. Cracking in the concrete embedded stud cannot be readily detected by non-destructive tests.

In contrast, the tests on coiled spring pins, showed that fatigue failure is characterised by gradual loss of load capacity with cracking at different locations in the pin. Also, the bore of the pins can be inspected for fatigue cracks and additional pins added nearby if necessary. It was therefore concluded that a 10% probability of failure could be accepted for fatigue failure of a coiled spring pin, provided a limit of 2mm was imposed on permanent slip under repeated service loading.

The test results obtained for 20mm diameter pins and the mean and 10% design lines are compared in Figure 5 with the mean and 2.3% design P-N relationship for 19mm welded studs recommended in BS5400 Part 10. From this, it can be seen that the fatigue endurance of 20mm diameter pins is better than that of 19mm welded studs at $N < 10^6$ cycles and, at 10^7 cycles, the maximum range of design shear load is 18.8 kN compared with 20.7 kN for a 19mm stud (ie about 10% lower).

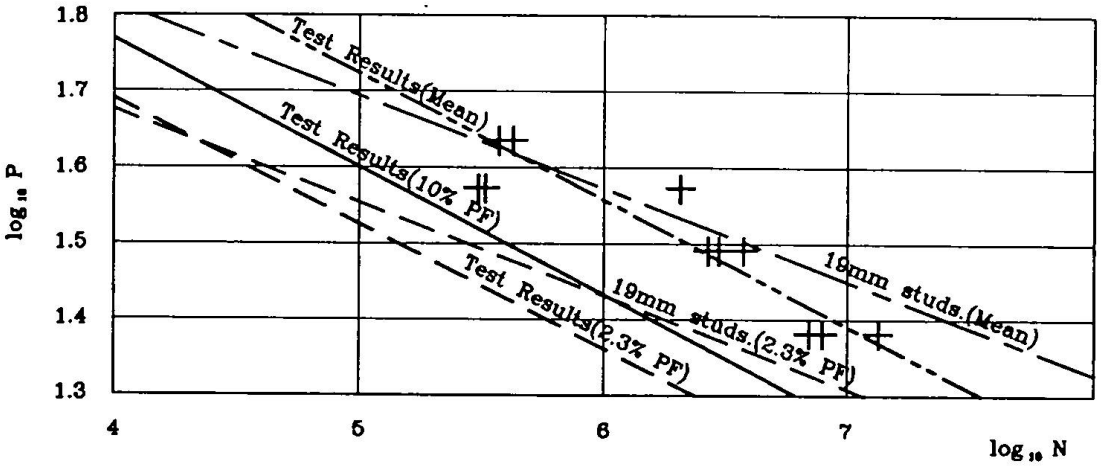

Figure 5 Load-Endurance Relationships for Coiled Spring Pin Connectors

6. Recommended Design Criteria

From the test results which have been obtained, the authors recommended that the following criteria for heavy duty 20mm coiled spring pin connectors could be adopted for the design for pin connectors installed in the Grade 37.5 concrete and 25-35mm thick steel flange plates in the Canadian box girder structure:

i) The nominal static strength of a pin, P_u, can be taken as 130kN

ii) The design fatigue endurance can be determined from the relationship

$$\text{Log}_{10}N = 14.767 - 6.1 \text{ Log}_{10}P$$

The above endurance relationship may be dependent on the fit of pins in the holes. In the tests, the mean interference fit was tighter than recommended by the pin manufacturer (see Table 1)

but the hole sizes in the specimens were representative of those achieved on site (see Section 7 below).

	Hole Diameter			Pin Diameter			Mean
	Min	Max	Mean	Min	Max	Mean	Interference
Manufacturer's Data	19.85	20.25	20.05	20.40	21.00	20.70	0.65
Test Specimens (Steel)	19.92	20.14	20.00	20.75	21.01	20.88	0.88
Test Specimens (Concrete)	19.96	20.25	20.04	20.75	21.01	20.88	0.84

Table I Comparison of Manufacturer's Specification with Test Specimens

7. Use of Coiled Spring Pin Connectors for Upgrading the Fatigue Endurance of an Existing Structure

The design values obtained from the tests described in the paper were adopted for upgrading the fatigue life of a multi-span composite box girder rapid - transit guideway structure in British Columbia, Canada. The retrofit contract consisted of drilling close-tolerance holes through the steel top flange and concrete deck of an open-top steel box girder and installing approximately 2500 coiled spring pins over a six month period with no interruption to transit service. The jacking force required for installation of the pins varied from 62 to 205kN.

The specification called for hole diameters to be from 19.85 to 20.25mm with a maximum diameter difference at the steel/concrete interface of 0. 1 mm. This required careful design and operation of the drilling equipment by the contractor. The profiles of all holes were measured and recorded. Table 2 summarises the results of the holes drilled in the structure. Only 14 holes with measured diameters in the range 20.26 to 20.30mm failed to meet the specification. The pins in these holes were abandoned and new holes were drilled for replacement pins. The majority of pins were installed from inside of the box girders but, where the minimum spacing of 100mm could not otherwise be maintained, some pins were positioned from the outside. After installation, the heads of the pins were sealed to prevent moisture ingress.

Girder	Element	Diameter of Hole (mm)			Standard
		Min	Max	Mean	Deviation (mm)
Outbound	Steel flange	19.90	20.28	20.07	0.07
	Concrete	19.90	20.75	20.07	0.08
Inbound	Steel flange	19.90	20.30	20.09	0.07
	Concrete	19.88	20.30	20.07	0.08

Table 2 Hole diameters achieved in retrofit contract

The transit authority is currently considering using the same method to upgrade another section of steel-composite guideway. The principal advantage of using coiled spring pins for fatigue strength enhancement is that they provide an unobtrusive, non-disruptive system for which design rules based on test data are now available. In addition, the pins can be periodically inspected for fatigue cracks and can easily be augmented if required.

The authors gratefully acknowledge the consent of BC Transit to publish this paper.

Ultimate Strain and Strength of RC Columns Retrofitted by Steel Tubes

Kenji SAKINO
Professor
Kyushu University
Fukuoka, Japan

Kenji Sakino, born 1946, received his PhD from Kyushu University in 1982. His research interests include earthquake resistance of reinforced concrete columns and shear walls, confinement of high-strength concrete, and inelastic behaviour of concrete-filled steel tubular columns.

Yuping SUN
Research Associate
Kyushu University
Fukuoka, Japan

Yuping Sun, born 1958, received his PhD from Kyushu University in 1992. His research interests include seismic behaviour of reinforced concrete columns, confinement of high-strength concrete, and non-linear analysis of concrete members.

Amin AKLAN
Graduate Student
Kyushu University
Fukuoka, Japan

Amin Aklan, born 1958, completed his ME degree in structural engineering at Kyushu Univ. in 1995. He is currently a doctoral student in graduate school of engineering at Kyushu Univ.

Summary

Ten reinforced concrete columns retrofitted by square steel tubes were tested under combined bending moment and constant axial load to investigate the main factors influencing ultimate strain and ultimate moment of the retrofitted R/C columns. Test results indicated that the ultimate strains of extreme concrete fiber at maximum moment were not constants, but varied mainly according to wall thickness of the steel tubes. Test results also showed that ultimate strength of the retrofitted columns increased as wall thickness of the steel tubes and the axial load increased.

1. Introduction

It is now well known that earthquake-resistant capacity of a reinforced concrete column can be remarkably enhanced when the column is encased or retrofitted by a steel tube. As compared with conventional transverse hoops, the steel tube has two more advantages of providing a large amount of transverse steel easily and preventing spalling of the shell concrete. Because of these merits, confining method utilizing the steel tube has been widely used to retrofit or strengthen existing concrete columns, particularly columns designed under previous Japanese design codes which nowadays are known to be unsound.

To establish a rational design method for the columns retrofitted by steel tube (referred to as tubed column hereafter), knowledge of the ultimate strain and strength of tubed column sections is of fundamental importance. In authors' previous study [1] of inelastic behavior of the tubed columns, ultimate strain and strength were only indirectly investigated through load-displacement responses of columns under axial load and bending moment with shear. For the columns under axial load and bending moment with shear, since the moment gradient and extra confinement from the end stiff loading stubs exist, it is hard to assess the actual ultimate strain and strength of tubed sections. Therefore, in order to better understand the real ultimate strain and strength of the tubed columns, experimental work on the tubed columns subjected to axial load and bending moment without shear is necessary.

The purpose of this paper is to experimentally study the effects of the axial load level and wall thickness of the steel tube on the moment-curvature relationship of square tubed columns without shear. A total of ten square reinforced concrete columns encased by square steel tubes available on the market were fabricated and tested under constant axial load and monotonic bending moment. Furthermore, based on a stress-strain curve model for the confined concrete proposed by authors,

Table 1 Details of the test columns and primary results

Specimen	fc (MPa)	B/t	Axial load		Test results			Theoretical results				
			N(kN)	n	M_m	ε_m	M_{cm}	ε_{cm}	M_p	ratio	M_{ACI}	ratio
T6S03	50.7	44	98	0.03	76	0.0046	NA	0.0065	65	1.17	64	1.19
T6S35			991	0.34	124	0.0148	122	0.0065	125	0.99	105	1.18
T6S50			1461	0.51	133	0.0112	131	0.0065	132	1.00	98	1.36
T6S70			1971	0.68	117	0.0068	116	0.0065	128	0.92	81	1.45
T6C50			1461	0.51	145	0.0061	144	0.0065	134	1.08	98	1.48
T9S03		30	98	0.04	76	0.0041	NA	0.0102	65	1.17	63	1.20
T9S35			941	0.34	133	0.0127	130	0.0102	123	1.08	100	1.33
T9S70			1883	0.68	152	0.0119	146	0.0102	145	1.05	76	2.01
T9S90			2501	0.91	146	0.0186	139	0.0102	133	1.10	28	5.27
T9C70			2050	0.74	174	0.0076	NA	0.0102	144	1.21	69	2.50

fc: Compressive strength of concrete cylinder
B/t: Width-to-wall thickness ratio of steel tube
N: Axial load applied
n: Axial load ratio
M_m: Experimental ultimate strength
M_{cm}: Experimental moment at ε_{cm}
ε_m: Ultimate strain of extreme concrete fiber at M_m
ε_{cm}: Theoretcal ultimate strain [3]
M_p: Ultimate strength calculated using the proposd stress block
M_{ACI}: Ulitmate strength calculated using the ACI stress block [2]

a stress block for estimating ultimate strain and strength of the tubed column is proposed.

2. Experimental Work

2.1 Specimens and Testing Method

Test specimens were 250x250x750mm prismatic columns with the same concrete strength and amount of longitudinal bars. A total of ten specimens were divided into two series, T6 and T9, according to wall thickness (6mm and 9mm) of the steel tubes used. Experimental variables among each series of specimens were axial load ratio and confining types of square steel tubes (split or continuous). Details and primary results of all specimens are listed in Table 1.

Longitudinal bars in each specimen consisted of twelve 13mm diameter (D13) deformed bars, which were welded to the end plates, to give a steel ratio of 2.69%. Confining steel tubes were provided by square steel tubes of 250x250x6mm and 250x 250x9mm available on the market. The yield strengths of the D13 deformed bar, T6 steel tube and T9 steel tube are 340MPa, 303MPa and 300MPa, respectively. Concrete with designed strength of 42MPa was made of Portlant cement and aggregate with a maximum size of 20mm. The average compressive strength of concrete cylinders during testing is given in Table 1.

Fig.1 shows the sectional details of specimens and the loading condition. In order for the steel tube not to directly sustain the axial stresses due to the axial load and bending moment, clearances of 10mm were provided between the steel tube and end steel plates at both ends of specimens. The steel tubes of four specimens (S-specimen) in each series were split into halves at the middle of the column, and a clearance of 10mm was provided between the two halves. This was to avoid any unexpected flexural stresses in the confining steel tubes during the bending action. For the fifth specimen (C-specimen), the steel tube was left intact to investigate the effect of continuity of the steel tube. The values of axial load ratio, defined as $N/A_c f_c'$, for the T6-series specimens were 0.03, 0.35, 0.50, and 0.70, while those of the T9-specimens were 0.03, 0.35, 0.70 and 0.90.

As shown in Fig. 1(b), the bending moment was exerted by pushing the loading beams through

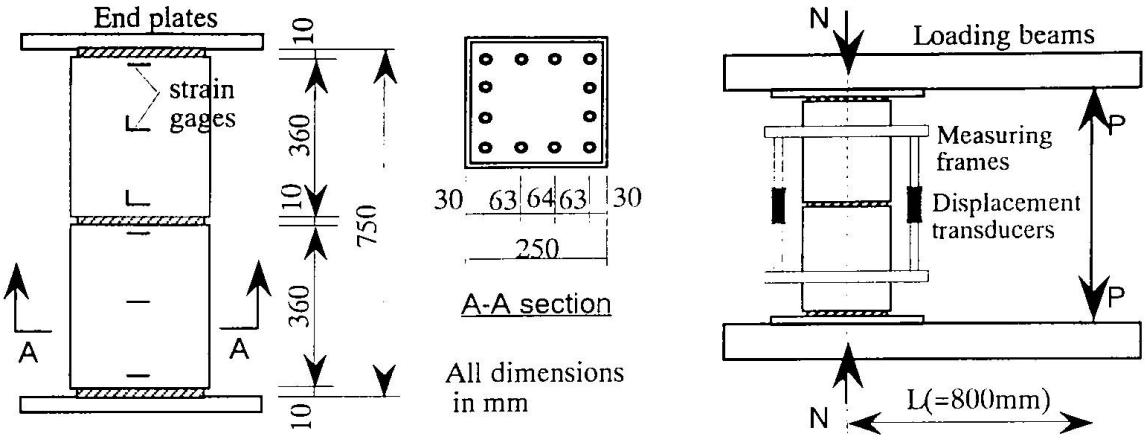

(a) details of specimens (b) loading condition

Fig.1 Details of specimens and loading condition

two hydraulic jacks after applying the axial load N. The axial load was applied by means of a 5MN universal testing machine, and was adjusted continuously so that the axial loads (N-P) in the specimens was maintained constant during the tests.

Strains were measured by 10-mm strain gages mounted on the compression and tension surfaces of the steel tubes. (See Fig. 1(a)). The average curvature over the central 500mm testing region of the specimen was measured by a pair of displacement transducers attached to measuring frames. Lateral deflection at the middle of the specimen was measured by a displacement transducer with reference to rotating centers to allow for the calculation of the secondary moment caused by the axial load N.

2.2 Experimental Results

Experimental results of the ultimate strength M_m and the corresponding ultimate strains of extreme concrete fiber ε_m are listed in Table 1. Fig. 2(a) and (b) shows the moment-curvature relations and the moment-ε_{ce} relations, respectively. In Fig. 2, ε_{ce} denotes compression strain of extreme concrete fiber, and the open squares and solid squares represent the testing stages when moment-curvature curves reached their peaks and when the steel tubes contacted the end plates, respectively. The dotted lines superimposed in moment- ε_{ce} curves express the theoretical ultimate strains ε_{cm}, which will be described in the following section. Experimental bending moments corresponding to the theoretical ε_{cm} are listed in Table 1 as M_{cm}.

It will be seen from Fig. 2 that specimens of T6 and T9 series exhibited very stable behavior even under such a high axial load as n=0.7 and n=0.9, respectively. Higher ultimate strength was observed in specimens encased by the steel tube with 9mm wall-thickness. On the other hand, in specimens under very low axial load, T6S03 and T9S03, effect of the wall thickness on the ultimate strength was not remarkable. Because low axial load results in small compression area, hence the ultimate strength is less sensitive to the confinement degree of steel tubes.

As obvious in Table 1, the experimental ultimate strains at extreme concrete compression fiber ε_m showed a large scattering and varied from 0.004 to 0.019, much higher than the value of 0.003 as recommended in the ACI code [2]. The ultimate strains appear to be mainly affected by the wall thickness of steel tube, and no clear correlation existed between the ultimate strains and the axial

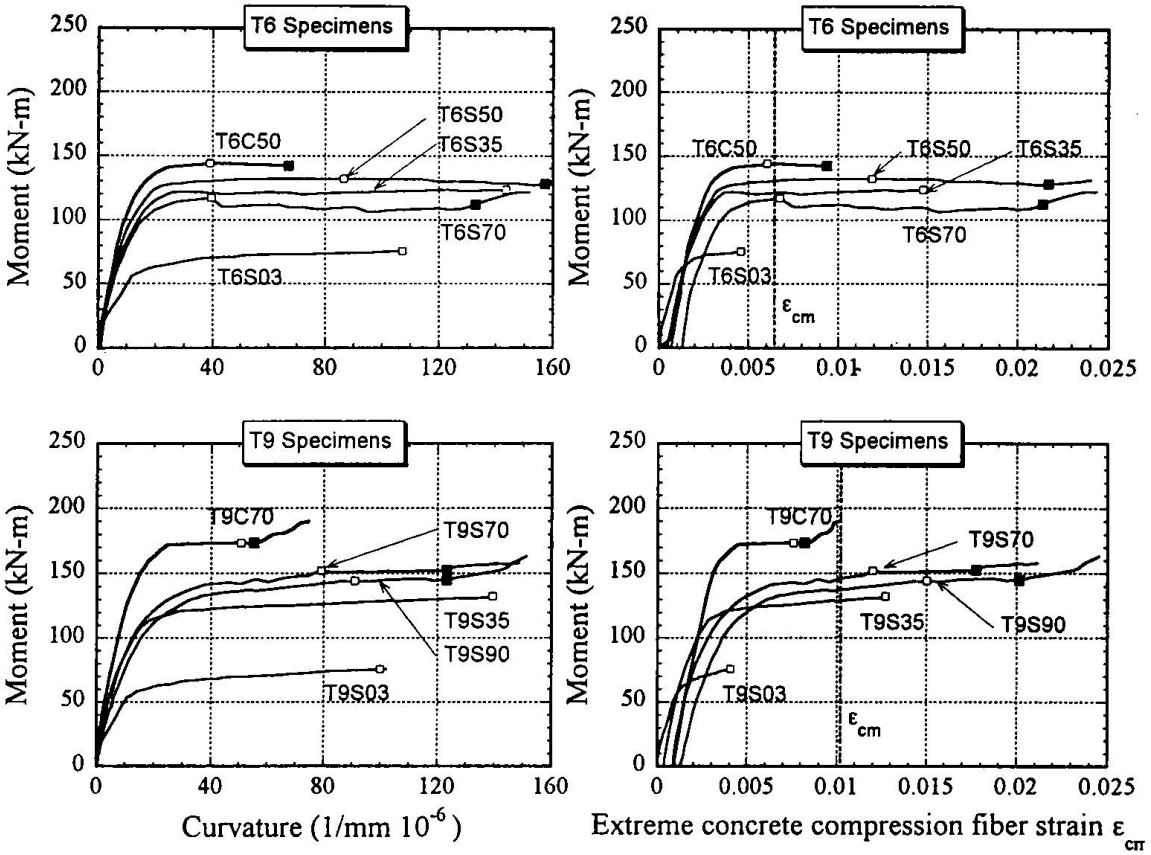

(a) moment-curvature relationships (b) moment-ε_{ce} relationships

Fig.2 Experimental results

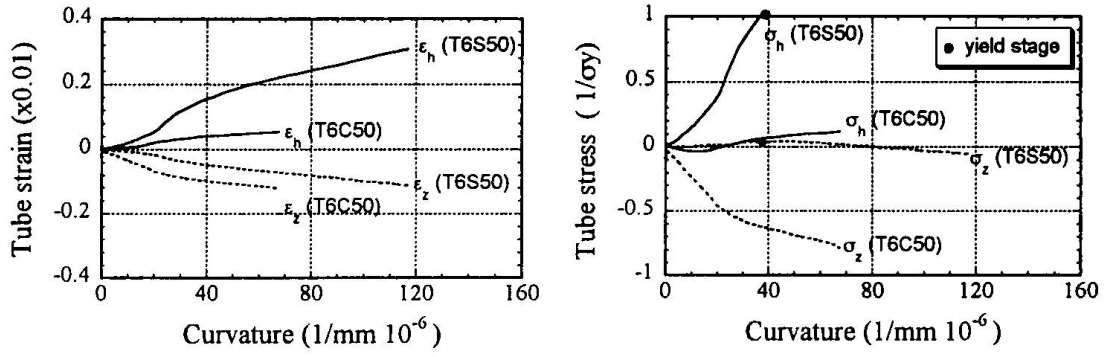

(a) tube strain-curvature relationships (b) tube strain - curvature relationships

Fig. 3 Strain and stress states in the steel tubes

load levels. It can also be seen from Table 1 that the experimental moments M_{cm} at the theoretical ε_{cm} closely approximated the experimental ultimate strengths M_m. Therefore, instead of a experimental formula for ε_m, it is reasonable to utilize the theoretical ε_{cm} for estimating the ultimate strength.

By comparing test results of two pairs of specimens, T6S50 and T6C50, and T9S70 and T9C70, it can be seen that the C-specimens exhibited higher ultimate strengths than S-specimens. To

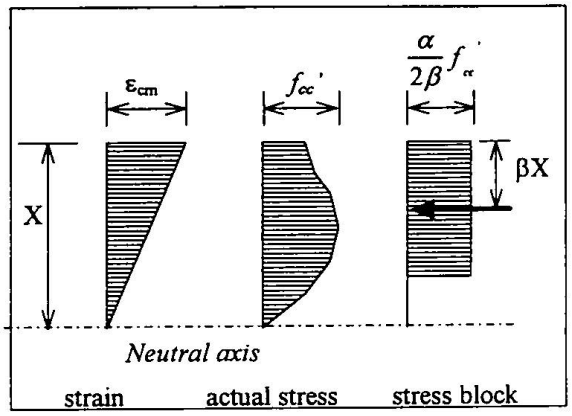

(a) distributions of strain and stress

$$\frac{\varepsilon_{cm}}{\varepsilon_{co}} = 1.375 + 0.108K - 0.102K^{-4}\left(\frac{f_c'}{42}\right) \quad (1)$$

$$\alpha = 0.724 + 0.107K - \frac{0.037}{K - 0.007}\left(\frac{f_c'}{42}\right) \quad (2)$$

$$\beta = 0.383 + 0.046K - \frac{0.019}{K + 0.387}\left(\frac{f_c'}{42}\right) \quad (3)$$

$$K = \frac{f_{cc}'}{f_c'} = 1 + 11.5\frac{\rho_t f_{yt}}{f_c'}\left(\frac{t}{B - 2t}\right) \quad (4)$$

$$\frac{\varepsilon_{co}}{\varepsilon_o} = \begin{cases} 1 + 4.7(K - 1), & K \le 1.5 \\ 3.35 + 20(K - 1.5), & K > 1.5 \end{cases} \quad (5)$$

(b) parameters for the stress block

Fig. 4 The proposed stress block

investigate the reason for this phenomenon, the strain and stress states of steel tubes for these specimens were examined. Fig. 3 shows experimental results of the T6 specimens only, since the T9 specimens had similar results. Fig. 3 shows the lateral strains ε_h and axial strains ε_z of the steel tube measured on the compression surface at the middle of the specimens. The lateral stresses σ_h and axial stresses σ_z were calculated following Hook's law from measured ε_h and ε_z. Solid circles in Fig.3(b) express the stage when the steel tubes reached Von Mises' yield criterion.

For S-specimen encased by split tube, the ε_h was about three times of the ε_z , and the lateral stresses σ_h were predominant, which means that the steel tube mainly acted as a lateral confiner. On the other hand, the ε_z in continuous tube of the C-specimen showed larger values than the ε_h. The axial stresses σ_z became predominant, which implies that the steel tube in C-specimen mainly sustained the axial stress incurred during the bending process. Therefore, it is necessary to cut the continuity of the steel tube when experimentally studying confinement effect of the steel tube.

3. Theoretical Work

3.1 Stress Block and Ultimate Strain

It is well known that ultimate strength of a reinforced concrete section can be simply calculated by utilizing the stress block of the compressed concrete. As apparent in Table 1, however, the widely used ACI stress block resulted in very conservative estimation of ultimate strengths of the tubed columns because of conservative nature of the ultimate strain of 0.003 as well as ignorance of confinement effect of the steel tube in the ACI stress block. To calculate the ultimate strength of a tubed column section more accurately, a new stress block, where confinement effect of the steel tube can be taken into consideration, is proposed in this section. Fig. 4 shows details of the proposed stress block and expressions for related parameters, the ultimate strain ε_{cm}, α and β.

Generally, expressions for α and β corresponding to any strain at extreme concrete fiber ε_{ce} can be derived by equalizing the axial force and moment of the stress block with that of the actual stress distribution. However, when evaluating ultimate strength, expressions corresponding to the specific strain at peak of moment-curvature curve are desirable rather than the general ones.

Based on authors analytical work on the moment-curvature behavior of the confined concrete section[3], Eq.1 was derived to estimate the ultimate strain ε_{cm}, Eqs.2 and 3 to evaluate parameters α and β. The process for developing Eq.1 through Eq.3 can be found elsewhere [3].

In Eq.1 through Eq.5, K=ratio of confined concrete strength to unconfined cylinder strength, a factor representing confinement degree of steel tube[4]; $\varepsilon_o = 0.94(f_c')10^{-3}$; f_c'=concrete cylinder strength; ρ_t=volumetric ratio of steel tube; f_{yt}=yield stress of steel tube; B and t=width and wall thickness of steel tube, respectively. Note that stresses f_c' and f_{yt} in Eq.1 through Eq.5 are in MPa.

3.2 Comparison Between Measured and Theoretical Ultimate Strengths

It can be seen from Table 1 that for S-specimens, the ACI strengths M_A are 18% to 427% conservative, while the ultimate strengths M_p obtained by using the proposed stress block predict experimental results very well. The measured ultimate strengths M_m exceeded the predicted results M_p only 6% on average for eight S-specimens. For specimens encased by continuous tube, the proposed stress block should not be applied to calculate the ultimate strength, since the steel tube in these specimens mainly sustained the axial stresses rather than acted as a lateral confiner.

4. Conclusions

The following conclusions can be drawn from the study reported in this paper on the ultimate strain and strength of the reinforced concrete column retrofitted by square steel tubes.

(1) When confined by square steel tube, the ultimate strain at extreme concrete compression fiber was not a constant, but varied from 0.004 to 0.019. Because of large scattering in the experimental ultimate strains and scarcity of test data, Eq.1 is proposed to predict the ultimate strain instead of developing an experimental formula for the ultimate strain. The fact that the experimental moments at the theoretical ε_{cm} closely approximated the ultimate strengths implies that Eq.1 would give reasonable results for design purpose.

(2) Ultimate strengths of the tubed columns increased with the increase of wall thickness of the confining tube. The increment in ultimate strength due to use of thicker tube becomes significant when the axial load level is high.

(3) A new stress block for the confined concrete is proposed to evaluate the ultimate strength of reinforced concrete columns retrofitted by square steel tubes(See Eq.1 - Eq.5). The theoretical ultimate strength predict the experimental result conservatively only by 6% on average.

References

[1] Sun, Y.P. and Sakino, K., "Flexural Behavior of Reinforced Concrete Columns Confined in Square Steel tubes," Procs. of the Tenth WCEE, Madrid, SPAIN, Vol. 8, July 1992, pp. 4365-4370.
[2] ACI Committee 318, "Building Code Requirements for Structural Concrete and Commentary - ACI 318-95," ACI, 1995, pp. 104-105.
[3] Sun, Y.P., Sakino, K., and Yoshioka, T., "Flexural Behavior of High-Strength RC Columns Confined by Rectilinear Reinforcement," J. of Struct. Constr., AIJ, No.486, Aug.1996, pp.95-106.
[4] Sakino, K. and Sun, Y.P., "Stress-Strain Curve of Concrete Confined by Rectilinear Hoops," J. of Struct. Constr., AIJ, No.461, July 1994, pp.95-104. (in Japanese)

Beams with Bonded-on Steel Plates: Design for Shear

Wim JANSZE
Assistant Researcher
Delft University of Technology
Delft, The Netherlands

Joop A. DEN UIJL
Senior Researcher
Delft University of Technology
Delft, The Netherlands

Joost C. WALRAVEN
Professor
Delft University of Technology
Delft, The Netherlands

Wim Jansze, born in 1966, graduaded in civil engineering from the TUD in 1993. Till May 1997 he worked as assistant researcher at the Stevin Laboratory on structural members strengthened with externally bonded steel plates.

Joop den Uijl, born in 1947, obtained his civil engineering degree in 1972 at TUD. In 1972 he joined the Stevin Laboratory for research. Currently, he works as a senior researcher on bond-related topics.

Joost Walraven, born in 1947, received his degree in civil engineering in 1972 at TUD, in 1980 his doctor degree by research on aggregate interlock. Since 1989 he is professor of the Concrete Structures Group.

Summary

A fictitious shear span is formulated for members without web reinforcement which are partially strengthened with externally bonded steel plates. An analytical expression for this fictitious shear span is derived based on tests and simulations. Then, by using MC90, the resistance by plate-end shear for partially plated members is calculated. In addition, for fully plated members the flexural-shear resistance is calculated with Rafla's formulation. Kani's shear valley for plate-end shear indicates that this type of behaviour dominates flexural shear.

1. Introduction

In practice, strengthening of RC members with externally bonded steel plates has mainly been applied in order to improve their flexural capacity. But how does the additionally bonded flexural reinforcement influence the shear resistance of the member? Oehlers [1992] investigated the shear resistance of members without web reinforcement by varying the "unplated length of the shear span." However, due to the scatter of test results the influence was not clearly shown.

Formulations for the mean value of the ultimate shear stress τ_{um} for conventionally RC members without web reinforcement were given by Rafla (Eq. (1)) and MC90 (Eq. (2)). After statistical analyses it emerged that for $C_{m,\,Rafla} = 0.85$ and $C_{m,MC90} = 0.18$ good agreement with test results on the ultimate nominal shear stress is obtained (Jansze [1997]). Then, the shear load V_{um} is simply calculated by multiplying τ_{um} with bd. These formulations and a formulated fictitious shear span for plate-end shear form the basis for a design method for plated members loaded in shear.

2. Analyses of variables influencing the shear capacity

2.1. Framework of the research study

At the Delft University of Technology a research study was conducted in which the influence of the unplated length L, the plate reinforcement ratio ρ_p (by varying plate width and thickness) and the shear span a were investigated (Jansze [1997]). The test set-up provided a shear span of 800 mm. The specimens were 100×200 mm^2 in cross section and contained two longitudinal 8 mm diameter ribbed bars at an effective depth of 170 mm. No web reinforcement was applied.

Rafla Eq. (1)	CEB-FIP MC90 Eq. (2)
$\tau_{um} = C_{m,Rafla}\ \alpha_u \sqrt{f_{cm}}\ \sqrt[3]{\rho_0}\ d^{-0.25}$	$\tau_{um} = C_{m,CEB}\ \sqrt[3]{3\frac{d}{a}\left(1+\sqrt{\frac{200}{d}}\right)\sqrt[3]{\rho_0\ f_{cm}}}$
$\alpha_u = 6.0 - 2.2\frac{a}{d}$ for $1.0 < \frac{a}{d} < 2.0$ $\alpha_u = 0.795 + 0.293\left(3.5 - \frac{a}{d}\right)^{2.5}$ $2.0 < \frac{a}{d} < 3.5$ $\alpha_u = 0.90 - 0.03\frac{a}{d}$ for $3.5 < \frac{a}{d}$	$V_{um} = \tau_{um}\, bd$ in which: ρ_0 = reinforcement ratio (=100A_s/bd) f_{cm} = mean compressive cylinder strength d = effective depth a = shear span

2.2. Experimental observations and numerical simulations on shear

Tests and numerical simulations showed a good agreement (Fig. 1). In the case of a fully plated specimen (L0), flexural-shear failure occurred in the shear span. The ultimate shear load was correctly calculated by Rafla's equation. However, when the shear span was only partially plated (L50, L100, L200), a large crack was initiated at the plate end in the unstrengthened part of the shear span. This crack developed into a shear crack at the onset of the ultimate load. Thus, failure is governed by plate-end shear. The FEM-simulations were carried out with DIANA. For concrete cracking the smeared crack model with bilinear tension softening was adopted.

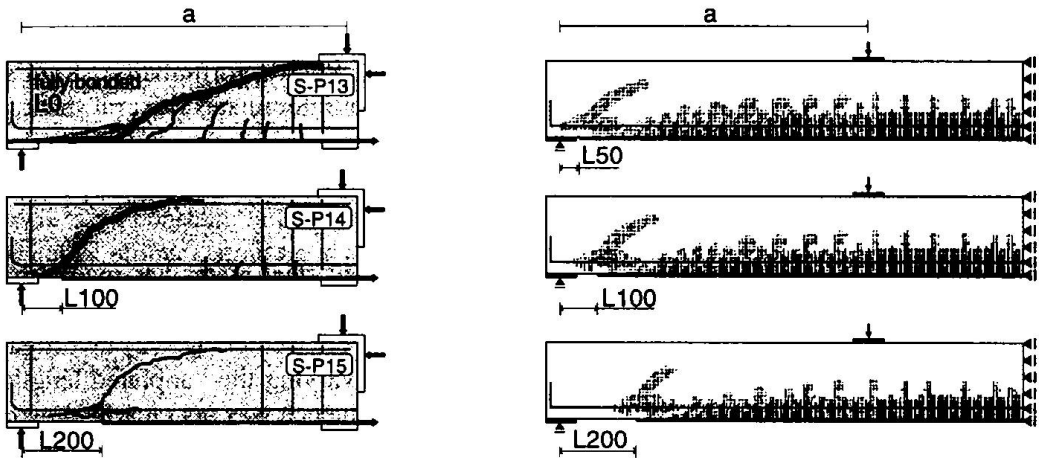

Fig. 1 Crack pattern after testing (left: L0, L100 and L200) and numerically calculated crack pattern at ultimate load (right: L50, L100, L200) of strengthened member with 5×100 mm² plate

2.3. Qualification of variables

When the results obtained from the experiments and the numerical simulations are graphically represented , the following conclusions with respect to the variables can be drawn:

- The unplated length L mainly governs the magnitude of the ultimate shear load, see Fig. 2. From about unplated lengths larger than 300 mm a combined shear-flexural peeling occurs;
- The shear span a has no influence on the ultimate shear load if $a > L+d$, see Fig. 3;
- The amount of plate reinforcement ρ_p (by varying cross sectional area) has little effect on the ultimate load by plate-end shear compared with flexural shear (L0), see Fig. 4.

Flexural shear can be described with conventional formulas in contrast to plate-end shear. For the derivation of an analytical expression to describe the shear resistance by plate-end shear, only the influence of the unplated length L is taken into account.

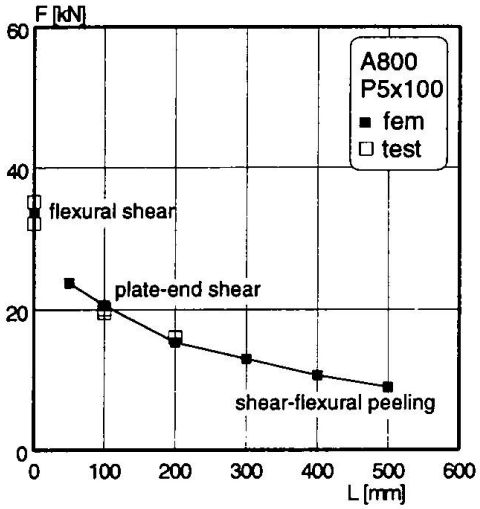

Fig. 2 Influence of unbonded length L on shear capacity

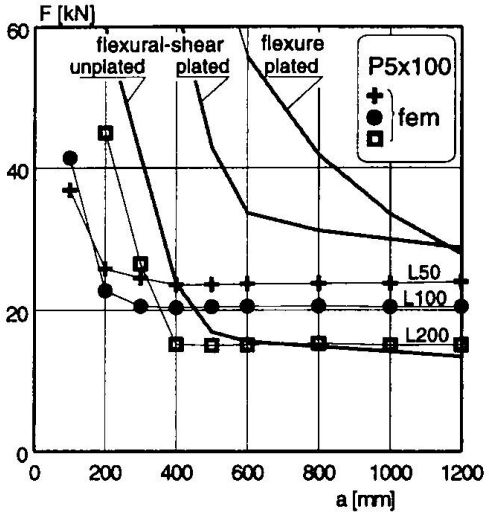

Fig. 3 Influence of shear span a on shear capacity as a function of L

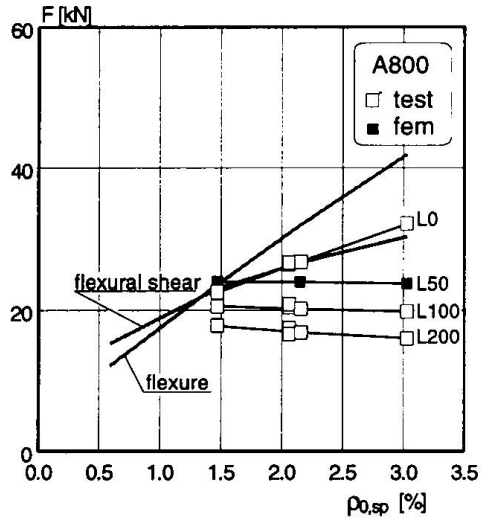

Fig. 4 Influence of reinforcement ratio $\rho_{0,sp}$ on shear capacity as function of L

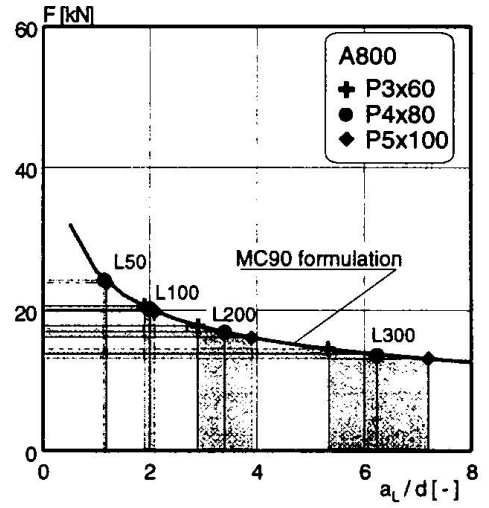

Fig. 5 Fictitious a_L /d according to tests and calculations on basis of MC90

3. Formulation for predicting the plate-end shear capacity

3.1. Additional parameter: fictitious shear span a_L

The plate-end-shear crack prevents the partially plated specimen to take full advantage of arch action due to intersection of the compressive-force path. Thus, only the contribution of beam action can be accounted for. When the ultimate shear loads of the partially plated members are compared with the shear resistance formulation of MC90 - which insufficiently takes full arch action into account compared to Rafla's equation (see Jansze [1997]) - a fictitious shear-span-to-depth ratio can be defined, see Fig. 5. Because the effective depth d_x of the unplated part is constant, a fictitious shear span a_L can be deduced, see Table 1. From this Table it follows that the fictitious shear span a_L increases with increasing unplated length L. At the same time, the

fictitious shear span also increases with increasing cross sectional area of the steel, however, this will be neglected. Note that the real shear span a of the member is 800 mm.

Table 1 Fictitious shear span a_L deduced from ultimate plate-end-shear loads and MC90

	L60		L100		L200		L300	
	a_L/d [-]	a_L [mm]	a_L/d [-]	a_L [mm]	a_L/d [-]	a_L [mm]	a_L/d [-]	a_L [mm]
P3x60	1.1	187	1.9	325	2.9	495	5.3	901
P4x80	1.15	195	2.0	340	3.4	580	6.2	1054
P5x100	1.2	205	2.1	355	3.9	665	7.2	1225

3.2. Modelling analogy

By introducing the fictitious shear span an analogy was found with Kim & White [1991]. There, an analytical expression was developed for predicting the location of the critical shear crack on the basis of ρ, a and d . Because limited data was available on the exact location of the critical crack position a_c, a statistical analysis resulted in Eq. (3), see Fig. 6 (left) (note: $\rho = \rho_s = A_s/bd$).

If RC members are partially strengthened by means of externally bonded steel plates, it was demonstrated that a plate-end-shear crack is forced to occur in the unplated part of the shear span. Hence, the position of the unbonded length L is fixed and equals to location of the critical shear crack a_c of Kim & White. Accordingly, the fictitious shear span a_L is analogous to the shear span a belonging to a_c. Then, Eq. (3) can be interpreted as Eq. (4), see also Fig. 6 (right).

$$a_c = 3.3\left[\frac{\rho\left(\frac{d}{a}\right)^2}{\left(1-\sqrt{\rho}\right)^2}\right]^{1/3} a \quad \text{Eq.(3)} \qquad \text{modelling analogy} \Rightarrow \qquad L = 3.3\left[\frac{\rho_s\left(\frac{d_s}{a_L}\right)^2}{\left(1-\sqrt{\rho_s}\right)^2}\right]^{1/3} a_L \quad \text{Eq.(4)}$$

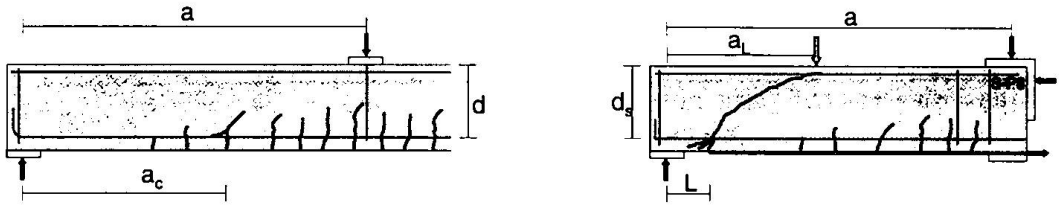

Fig. 6 Location a_c of governing flexural-shear crack according to Kim & White [1991] Modelling analogy with fictitious shear span a_L and unplated length L for partially plated member according to Jansze [1997]; plate-end-shear crack is analogous to flexural-shear crack

3.3. Verification and formulation of shear resistance by fictitious shear span

The fictitious shear span a_L as expressed by Eq. (4) is used to compute the shear resistance on the basis of MC90. Essential is that in this formulation the unstrengthened part is considered, so the effective depth of the internal reinforcement d_s and the internal reinforcement ratio ρ_s have to be considered. In Fig. 7 the computed shear resistance is compared with the experimental and numerically simulated results. It can be seen that the constant 3.3 of Kim & White overestimates the plate-end-shear load. However, analyses show that by replacing the constant 3.3 in Eq. (4) by the fictitious-shear-span-to-depth ratio a_L/d_s, good agreement is obtained between the plate-end-shear loads based on the fictitious shear span and the experimental and numerical results,

see Fig. 7. Thus, by substituting constant 3.3, Eq. (4) can be rewritten into Eq. (5) that explicitly expresses the fictitious shear span a_L :

$$a_L = \sqrt[4]{\frac{\left(1-\sqrt{\rho_s}\right)^2}{\rho_s} d_s L^3} \qquad \text{Eq. (5)}$$

For L50, L100, L200 and L300 a fictitious shear span of respectively 235, 395, 665 and 900 mm is calculated. These values are very satisfactory when compared to Table 1. Then, when the fictitious shear span calculated by Eq. (5) is subsequently used to calculate shear according to MC90, the plate-end-shear loads are in good agreement with the tests and simulations. When Eq. (5) is used to calculate the shear resistance of various concrete member geometry's as listed in Table 2, it is concluded that the analytical expression in combination with MC90 is definitely capable of calculating the plate-end-shear load of partially strengthened members. This method is applicable for a > L+d. Furthermore, Jansze [1997] shows that this method is also applicable to determine a lower bound for shear peeling loads, and not applicable for shear-flexural peeling.

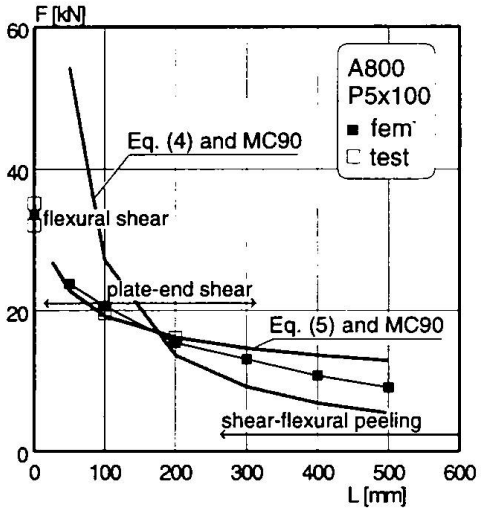

Fig. 7 Shear resistance of tests, simulations and according to model

Tests Jansze [1997]	series S-W	series S-H
A_c [mm²]	200x200	100x400
$\rho_{d,0}$ [%]	0.59	0.662
P [mm²]	5x100	5x100
L [mm]	100	200
a [mm]	800	1600
a_L [mm]	395	795
V_{exp} [kN]	35.9 / 36.5 35.8 / 36.9	38.1 / 40.6 40.3 / 34.4
V_{um} [kN]	37.7	36.5

Table 2 Shear resistance of additional tests according to fictitious shear span and MC90

4. Shear - Flexure interaction represented by Kani's shear valley

4.1. Input parameters for a case study

A case study is carried out in which the shear-flexure interaction is analysed by constructing Kani's shear valley for fully and partially plated members. For various shear-span-to-depth and reinforcement ratios the ultimate shear moment over ultimate flexural moment is calculated. A maximum value of $M_{Vcu} / M_{flex} = 1$ is adopted to indicate flexural failure. The case study is based on a member 100x200 mm² in cross section and the amount of external plate reinforcement is assumed to be equal to the amount of internal bars ($\rho_s = \rho_p$). Flexural failure is calculated by adopting yield stresses of 600 N/mm² and 285 N/mm² for the bars and plate, respectively. The mean compressive cylinder strength is 36 N/mm². Is must be stressed that at the axes the total amount of reinforcement is based on the reinforcement ratio in the constant moment region ($\rho_s + \rho_p$) and furthermore that the real shear span *a* is plotted in the graph for *a/d*.

4.2. Flexural capacity versus flexural-shear and plate-end-shear resistance

Both flexural shear for fully plated members (L0) and plate-end shear for partially plated members (in this case study L = 100 and 200 mm) are graphically represented by Kani's shear valley in Fig. 8. It is clearly seen that for plate-end shear Kani's shear valley has much more depth than for flexural-shear failure. Particularly for shear-span-to-depth ratio's $a/d < 4$ or 5 plate-end shear dominates flexural shear. For shear spans smaller than approximately $a < L+d$ an arch can be formed between the load and the support because the plate-end-shear crack does not intersect the compressive-load path. Thus, a plateau is visible as in the original shear valley. The valley of the L200 member has less depth than that of the L100 member, see also Fig. 3. The L100 and L200 graphs further indicate that with increasing unplated length plate-end-shear also governs failure for larger a/d-values. The graphs clearly indicate that one should be careful with strengthening short deep beams. The reduction of the bearing capacity by plate-end shear may be considerable, specially for small a/d-values.

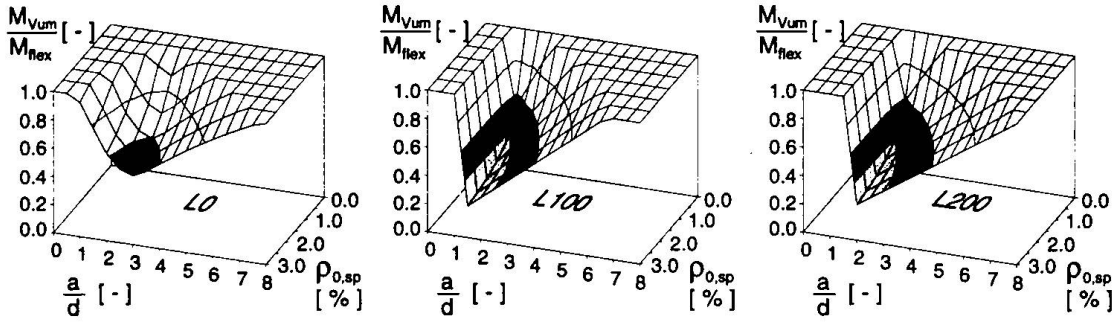

L0 -flexural shear *L100 - plate-end shear* *L200 - plate-end shear*

Fig. 8 Kani's shear valley for fully plated members and calculated Kani's shear valley for partially plated members with external steel plate stopped 100 and 200 mm short of the support

5. Conclusions

The fictitious-shear-span-to-depth ratio is successfully used in combination with the MC90 formulation on shear resistance to calculate the ultimate shear load for plate-end shear. Basically, the mechanism of plate-end shear is analogous to that of flexural shear, however, the ultimate shear loads differ significantly. Compared to the flexural capacity, up to about $a/d < 4$ or 5, failure by plate-end shear dominates failure by flexural shear. It is therefore advised to bond the steel plate as close as possible to the support to increase not only the flexural capacity, but also the shear resistance of the strengthened member.

Oehlers, D.J. [1992]. Reinforced concrete beams with plates glued to their soffits. *Journal of Structural Engineering*, Vol. 118, No. 8, August 1992, pp. 2023-2038.

Kim, W. and White, R.N. [1991]. Initiation of Shear Cracking in Reinforced Concrete Beams with No Web Reinforcement, *ACI Structural Journal*, V.88, No.3, May-June 1991, pp 301-308.

Jansze, W. [1997]. Strengthening with Externally Bonded Steel Plates: Design for Beam Shear and Plate Anchorage, *Dissertation*, Delft University of Technology, To be published in 1997.

Elastic Composite Construction between Timber and Wood-Based Materials

Hans HARTL
Civil Eng.
Holzbau Gmbtt
Vienna, Austria

born 1941.
1964: structural engineer in building companies in Germany and Austria
1971: receipt of civil engineer degree
1972: general partner and manager of the Building company Wenzl Hartl/Vienna
from 1978: activity as civil engineer
from 1980: professor for timber engineering at University of Innsbruck
from 1993: collaboration in various standards committees
from 1994: head of staff European Federation of Timber Construction.

Summary

Due to higher demands reconstruction of timber floors often request elastic composite construction between timber and wood-based materials. To commence construction, building or renovating it is necessary to uncover the existing timber beams. Afterwards sheathing panels (chip boards) are fixed to the beams with special connectors. A method of calculation and construction as well as the building process itself will be shown. This will be demonstrated with the example 'Salzburger Decke' ('Salzburg-type floor') in the ancient building 'Höllbräu' in the city of Salzburg.

1. Introduction

Many of the floors in old buildings are made of timber. These floors have not lost their workability through many centuries under dry conditions. However, dereliction and poor maintenance has lead to ingress of water and as soon as the moisture content in the timber elements increase the possibility of infestation by insects rises and then the wooden constructions may be destroyed within a short period. Today such structures are not completely demolished, but redeveloped due to the following reasons:

- Previous renovations of damaged timber beams in old and new buildings has not been executed correctly.
- Valuable and cultural antiquities and many examples of such losses (e.g. ceiling frescos or ceiling stucco) would be lost if the load-bearing timber beams are not restored properly are known.
- Recently the importance of construction substance especially in the old towns has been recognised and their preservation has been supported by politicians, sociologists and architects. Wherever possible the original floor load-bearing structures are to be maintained and not to be replaced by other building materials or structural members.

For these reasons the knowledge of the possibilities to redevelop timber floors are important.

2. Wood damage

Wood preservations have to be realised according to the degree of damage and will change from case to case. An overview of defects will be given, such as:

2.1 Defects related to living organisms

- Fungi
  - in living wood
  - in sawn timber
  - in timber in already erected structures
- Bacteria
- Insects
  - in living wood
  - in timber in already erected structures
- Marine pests

2.2 Other defects

- High temperatures
- Chemical defects
- Meteorological conditions
- Mechanical defects

3. Timber floors

3.1 Types of timber floors

At the turn of the last century types of timber floors in buildings in Austria were mainly the so-called 'Dippelbaumdecken' ('Dippel-tree floor') and later on 'Tramdecken' ('Beam floor') in the most cases with loose filling.

3.1.1 'Dippelbaumdecke' - 'Dippel-tree floor'

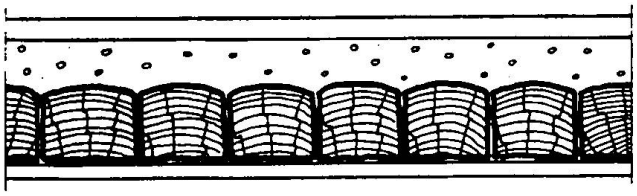

floor covering (e.g. marble)
bearing layer
pugging
dippel-trees (e.g. spruce logs)
reed matting
plaster

Fig 1 'Dippelbaumdecke' - 'Dippel-tree floor'

Belonging to the today's unusual 'dippel-tree floor' several 'dippels' (beams from logs) are situated side by side connected to each other with wooden dowels. The latter have the advantage that concentrated stresses are distributed on several 'dippels' and therefore the deflections and vibrations are reduced.

3.1.2 'Tramdecke' - 'Beam floor'
Several beams are spaced at app. 600 to 1000 mm depending on their cross-sections, spans and loading. In principle there are 'simple' and 'normal' floors. The 'simple' flooring lies on the beams directly and the 'normal' flooring (*see Figure 2*) floated on boarding joists in the loose

filling (pugging) which is supported by a lintel frame or pugging board fixed between the beams.

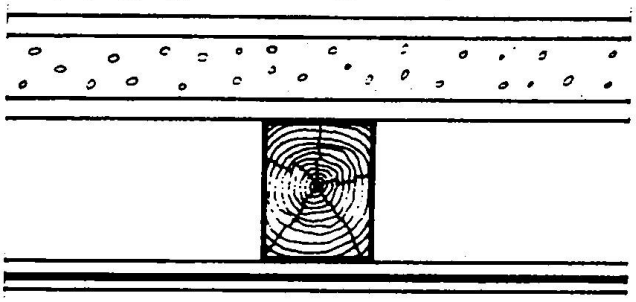

Fig 2 'Tramdecke' - 'Beam floor'

3.1.3 'Salzburger Decke' - 'Salzburg-type floor'

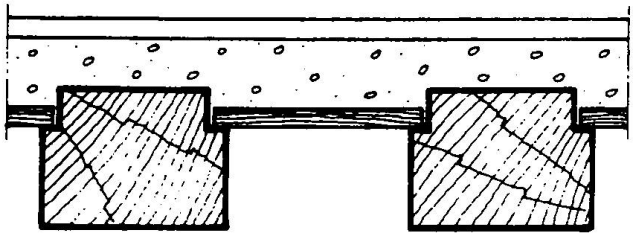

Fig 3 'Salzburger Decke' - 'Salzburg-type floor'

The cross-section of a beam is app. 270 and 270 mm and are spaced at app. 270 mm. Apart the edges of the beams are rebated to carry the pugging board which is doweled into place. The underside of the pugging board and the exposed faces of the beams are very often highly decorated.

3.2 Observation of wood damage

3.2.1 Exposed beams

In most cases these beams are exposed on at least three sides and therefore any defects are clearly visible.

3.2.2 Concealed beams

In practice concealed beams are widespread and it is necessary to expose them for inspection by the removal of the floor covering and loose filling. Only in this way a full report on the bearing construction and its condition can be prepared. Reasons for exposure of the beams are:

- Traditionally every fifth beam would be tied to or through the external walls to prevent spread by means of an iron strap and this has to be checked and the number increased if necessary.
- Large depths of loose filling have to be reduced to save dead weight and to allow for the increasing the capacity of payloads.
- Loose filling could become dangerous because of the accumulation of moisture or pests.
- The real extent of the damage can not often be established until a whole examination of the timber construction is possible.

- Without uncovering the construction elements any rehabilitation work is unpracticable.
- In the course of the restoration the building domestic services can be installed in the area of loose filling.

Therefore a hundred percent judgement of the timber construction as well as a repair or restoration is possible only in connection with total exposure.

The following expertise has to give answers to the question:

- relating to stability,
- assessment of serviceability (use of the rooms),
- constructional wood preservation, hot-air procedure, supported by chemical wood preservation if necessary,
- realisation of procedures for redevelopment.

4. Reconstruction

4.1 General

Fig 4 'Höllbräu' (view from 'Waagplatz')

Valuable historic timber constructions with localised defects should be renovated. To find the optimal solution how to repair it is necessary to have the exact knowledge of the kind of damage as well as the knowledge of previous attempts at refurbishment.

4.2 Example of reconstruction

The architectural aura of the city 'Salzburg' is mainly determined by its old buildings. In the middle of the city the ancient building 'Höllbräu' is located and is one of the oldest buildings. Its history traces back to the year 1377. After renovation it is now a high-class hotel. To increase the load bearing capacity and to reduce the deflections of the 'Salzburg-type floor' one possibility is to create the floor structure given in *Figure 6*. After the timber beams have been exposed, sheathing panels (flat chip boards) are connected to the beams with special nails. This floor structure represents an elastic composite construction between timber and wood-based materials.

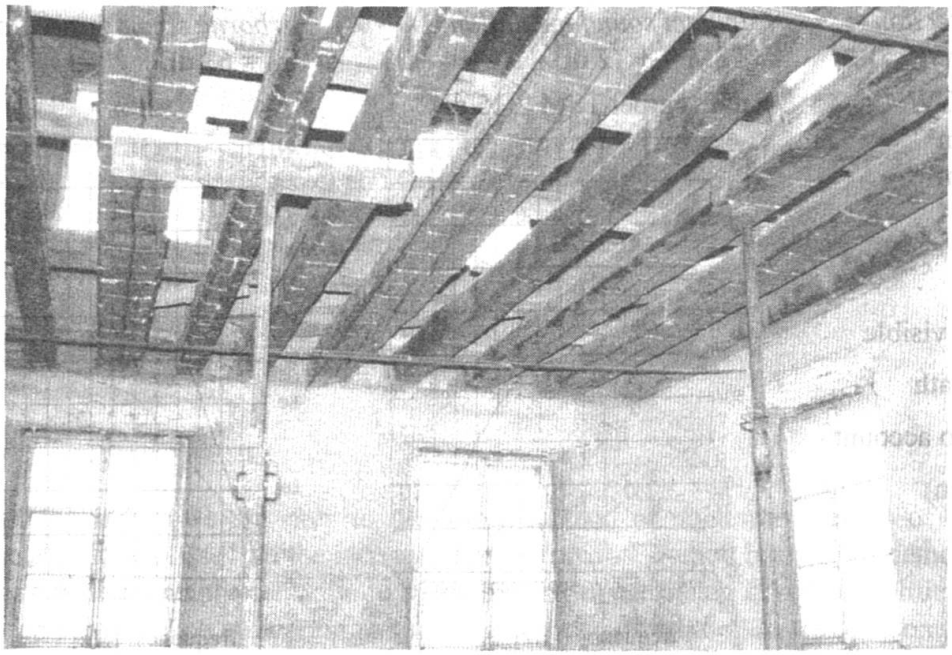

Fig 5 'Salzburger Decke' - 'Salzburg-type floor' after uncovering the existing timber beams

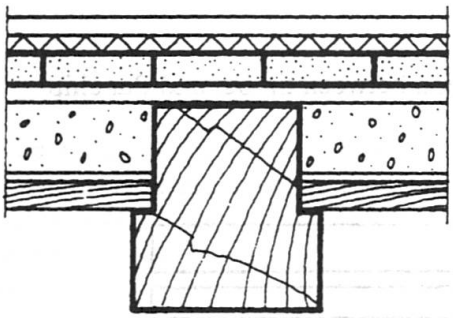

Flat chip board V 100, 25 mm (700 kg/m³)
Noise reduction mineral fibre
insulation elastic material 30/25
Concrete paving slabs 300x300x40, non-reinforced
Flat chip board V 20, 30 mm (700 kg/m³)
Loose filling 60 mm
Plaster board 25 mm
Wooden boards 40 mm (existence)

Fig 6 'Salzburger Decke' - 'Salzburg-type floor' after renovation

4.3 Standards

4.3.1 Resistance against fire
Classification of fire resistance has to be proved in accordance with national (ÖNORM, DIN, ...) respectively today with international standards (CEN-, ISO-Standards, Eurocodes, ...).
The 'Salzburg-type floor' after renovation complies to the requirements of the Austrian standard ÖNORM B 3800, Part 2 and to the more specific regulations of ÖNORM B 3800, Part 4.

4.3.2 Defects with respect to building physics
It is not surprising that the high demands in present standards with respect to thermal protection as well as to impact and airborne sound insulation are not obtained by the existing and insufficient former renovation. Local authorities now demand the removal of this 'deplorable state of affairs' by insisting that timber floors are therefore renovated by.
The valuable historic timber floors can be reinstalled over the new structure thereby maintaining the historic appearance of the building.

For verification see *Figure 7* and *Figure 8*.

Thermal Protection:
k = 0.38 W/m²/K
D = 2.41 m²K/W
m_{spu} = 45 kg/m²
m_{spo} = 37 kg/m²

Beams partly visible from underneath (not taken into account for verification)

Impact sound insulation:
TSM = + 12 dB
with carpet TSM ≥ 15 dB

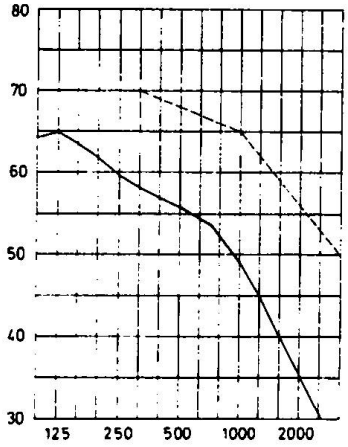

Fig 7 Impact sound insulation

Airborne sound insulation:
R_W = 63 dB

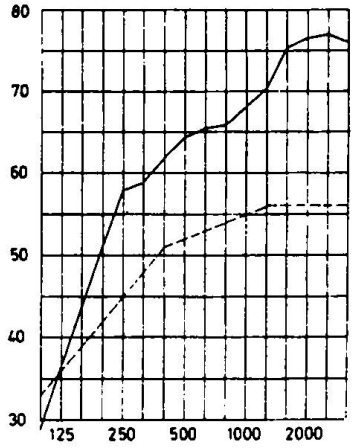

Fig 8 Airborne sound insulation

4.3.3 Calculation

Calculation was carried out with an elastic composite cross-section between timber and flat chip board including effective board width.

Static system:

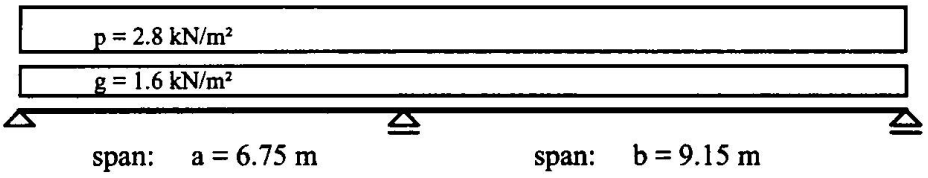

Bending moment line:

Shear stress line:

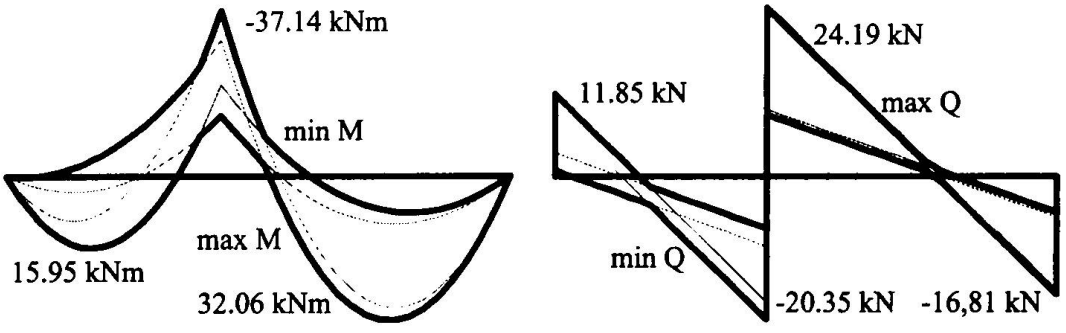

Fig 9 Static system, bending moment and shear stress lines

In conclusion the achievement of renovating of an old building in addition to the restoration work shown supplementary structural work is needed.

Hans Hartl

Strengthening of Composite Girder Bridge by External Prestressing

Ayaho MIYAMOTO
Prof., Dr. Eng.
Yamaguchi University
Ube, Japan

Minoru MOTOSHITA
Director and General Manager
Kyowa Sekkei CO., LTD.
Kobe Japan

Manabu FUJII
Prof. Dr. Eng.
Kyoto University
Kyoto, Japan

Summary

The aims of this paper are not only to develop a method of nonlinear analysis of prestressed composite plate girders based on the incremental deformation method but also to demonstrate the feasibility of the prestressing technique to strengthening of a existing composite girder bridge. A method of the performance evaluation and a design procedure of the prestressed composite plate girders with external tendons are proposed based on the analytical results considered with some optimum parameters which are geometric parameters and material parameters.

1. Introduction

The maintenance, repair, rehabilitation and strengthening of bridges in use around the world have been receiving more and more attention in recent years, and the deterioration of existing bridges due to increasing overloading and progressive structural aging has become a major problem. The number of heavy vehicles and volume of traffic using these bridges has come to exceed the values predicted at the time of bridge design, with the result that many of these bridges are suffering from fatigue damage and are now in urgent need of strengthening. In addition, problems can also be expected in providing suitable countermeasures for cases where revisions in the design live load exceed the present load capacity of the existing bridge. Prestressing technique can be considered as one effective method applicable in such cases[1][2]. At the same time, materials development is being actively pursued in such areas as high strength steels and continuous fiber reinforced plastics(FRP) that have high strength, outstanding corrosion resistance and high elasticity. If these materials can be successfully incorporated in prestressed composite structures, not only the strengthening of existing bridges, but the development of new bridge design configurations becomes possible. In this paper, in order to investigate the fundamental mechanical behavior of prestressed composite structures, a simply supported prestressed composite plate girder was made the subject of static behavioral analysis, taking such things as the cable arrangement and cable material as parameters. In addition, full scale tests were carried out on prestressed composite plate girders to confirm the results of the analysis. Also, with a view to evaluating methods of strengthening existing bridges, the fundamental characteristics of prestressed composite plate girders (hereafter PS composite girders), namely the yield load, ultimate load, and flexural rigidity, were evaluated. A method to improve load carrying capacity by introducing prestressing force is also proposed, based on the results of the various analyses. Also, as a numerical example, the results of applying the method to an actual bridge were studied to evaluate the performance.

2. Nonlinear Analysis of Prestressed Composite Girder and Verification Test

2.1 Fundamental Assumptions and Flow of the Analysis

The flowchart of the incremental deformation method, one means of carrying out the elasto-plastic analysis that can be applied in the case of the PS composite girder for various cable materials and arrangements, is shown in Fig. 1[3]. The details of the elasto-plastic analysis method used are described in the authors' papers[3] [4].

2.2 Outline of Verification Tests

Five test specimens were prepared for the verification tests, four PS composite girders with the queen post cable arrangement (two girders with cable within the cross section and two girders with cable arranged outside the cross section)[4], and a standard girder without cables. The specimens prepared were models of an actual composite steel plate girder bridge, the steel girder to concrete deck slab distribution ratio was made close to that of the actual bridge. As a result, the neutral axis within the elastic region of the girder lies just below the upper flange, and the cross section is very

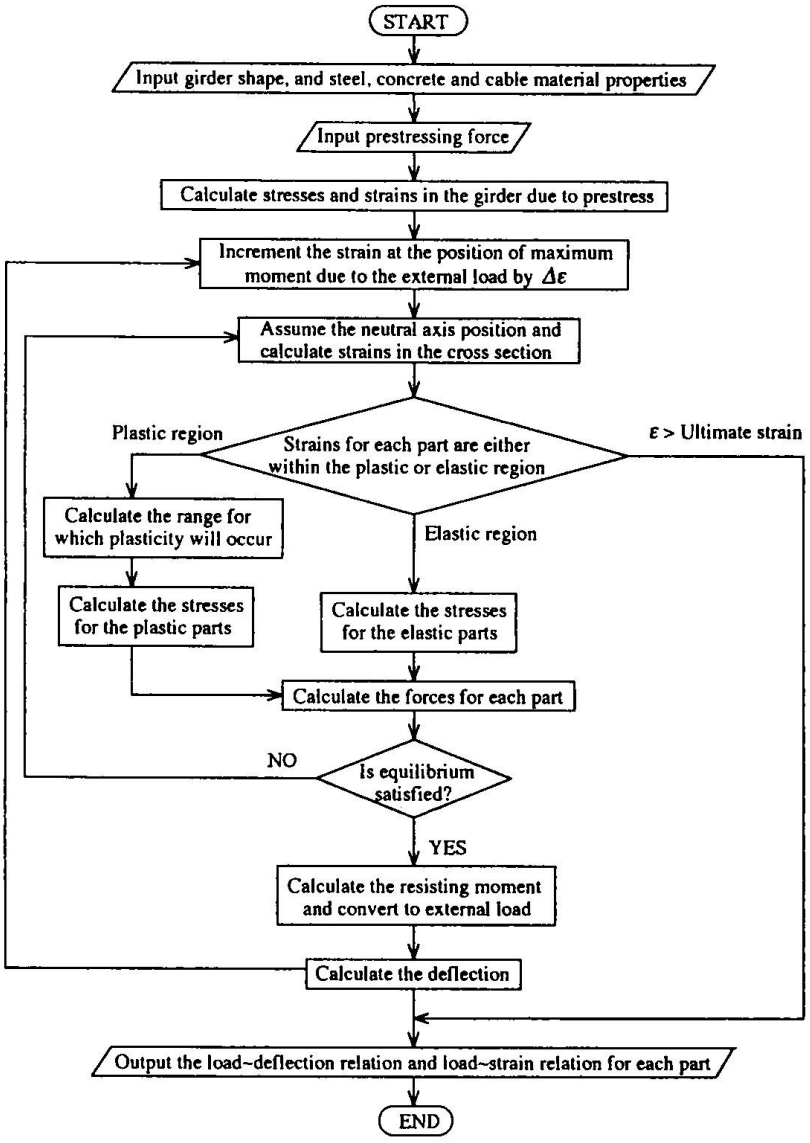

Fig. 1 Flowchart of incremental deformation method

similar to the main girder cross section of a general composite steel plate girder bridge. Commercially available H-section steel girder (SS400) was used[3], and two cable materials, PC steel cable and aramid fiber(braided cable) cable. A 50mm thick steel plate ground to form a circular arc and PVC pipe were incorporated at the position where the cable bends to provide smooth cable deflection. An outline of the different types of specimens is given in Fig. 2 and Table 1. The details of the verification method used are also described in the authors' papers[3] [4].

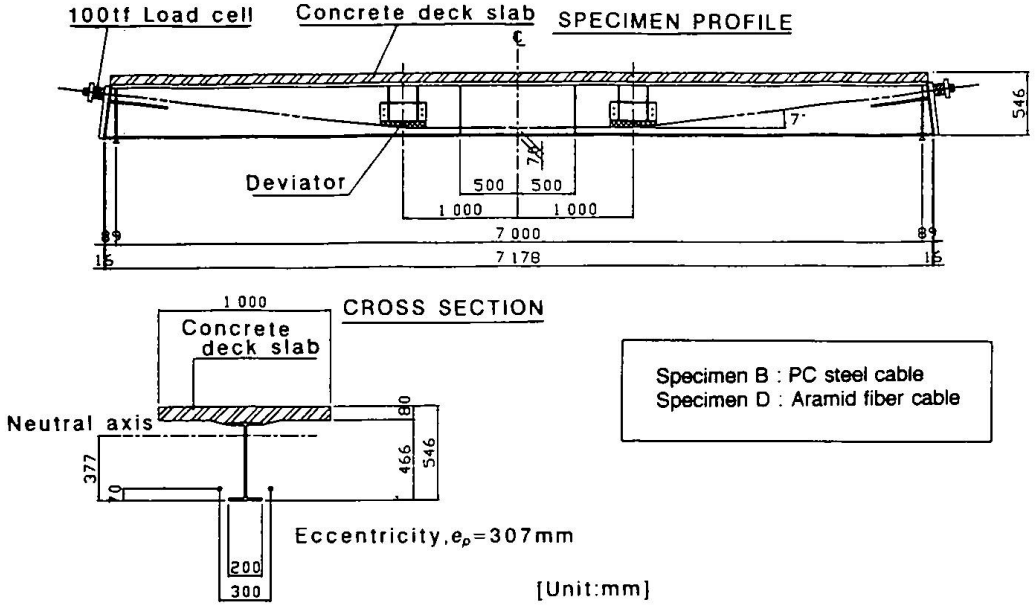

Fig. 2 Test specimen(for cables within the cross section)

Table 1 Types of specimen

Specimen	Cable arrangement	Type of cable	Initial prestressing force (Total of 2 cables, tf)
A	No cable	——	——
B	Queen-post type(Draped) Inside cross section	Steel strand	70.0
C	Queen-post type(Draped) Outside cross section	Steel strand	17.0
D	Queen-post type(Draped) Inside cross section	Aramid fiber strand	70.0
E	Queen-post type(Draped) Outside cross section	Aramid fiber strand	17.0

2.3 Comparison of Test and Analysis Results

The following results can be made on overall comparison of the test results and analysis results: i) Overall, good agreement was achieved for the behavior of the load-midspan deflection relation for the test specimens. However, the value of initial gradient for the test was lower than that obtained from analysis. This can be attributed to such factors as the effective width of the concrete deck slabs at the slab center and in the region of the support points being different, ii) Small discrepancies occurred between the values of yield load and ultimate load, however, good agreement can be seen in such trends as the higher yield load being achieved in the case of cables within the cross section than outside the cross section, and lower values of yield and ultimate load occurring for low values of elastic modulus, iii) Although differences occurred in the final values of increase in the cable tension due to the differences in ultimate load, good overall agreement was achieved between the test results and the results of the analyses.

3. Performance Evaluation and Strengthening Design

3.1 Parameter Analysis and Design Procedure

For the purpose of strengthening the existing bridges indicated below, the parameters having an effect on the mechanical behavior of the PS composite girder were selected as follows, (1) b/L : Length span ratio of the horizontal portion of the cable, (2) e'/y_{s1}: Ratio of the eccentricity at the cable attachment position to the distance, from the lower surface of the bottom flange to the composite girder neutral axis, (3) e/y_{s1}: Ratio of the distance from the cable attachment position to the cable horizontal portion, to the distance from the lower surface of the bottom flange to the neutral axis, (4) E_t/E_s : Ratio of the Young's modulus of the cable to the Young's modulus of the steel, (5) A_t/A_v : Ratio of the cable cross sectional area to the composite girder cross sectional area, A_c/A_s : Ratio of the concrete deck slab cross section to the steel girder cross section. And by means of a parameter analysis, an evaluation of the performance of the PS composite girder was made in relation to improving the yield load, ultimate load and flexural rigidity. An explanation of the various symbols of the analytical model used in the analysis and details of the cross section of the composite standard girder are given in Fig. 3. In here, the dimensionless parameters (1), (2) and (3) are related to the arrangement of the cables. The dimensionless parameters (4) and (5) are related to the cable materials. The cable materials considered are generally FRP, the stress-strain relationship was assumed to vary linearly up to the point of failure[4]. The dimensionless parameter (6) relates to thickness of the deck slab, the width of the deck slab was made constant and only the thickness varied.

Fig. 4 shows a proposed design procedure for strengthening by increasing the girder yield load, based on the parameter analysis in above mentioned.

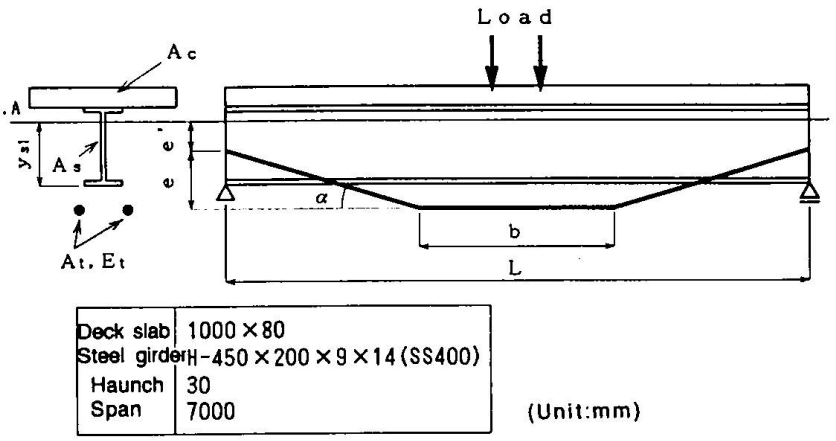

Fig. 3 Model symbols and section details used in parameter analysis

3.2 Numerical Example

In order to demonstrate the applicability of the method, a practical example of its application to the composite girder model of an actual bridge will be given. The bridge chosen for this was designed as a second class bridge(TL-14 load), and was a simply supported, single span, live load composite girder bridge, having 3 main girders. With the increase in traffic volume in recent years, the live load on the bridge is expected to increase to a level equivalent to that of a first class bridge. For this reason, it was decided to raise the standard of the bridge to first class bridge standard by a combination of bridge widening, the introduction of prestress, and increasing the thickness of the deck slabs. The purpose of the strengthening of this bridge is therefore to raise the class of the bridge from second to first class, in other words to increase the yield load. In order to satisfy this objective, it should be possible to apply a TL-20 load (*TL-14 × 1.43 approx.*) to the bridge without the stress in any of the bridge members exceeding the maximum allowable stress. The target value for the strengthening was set to give a yield load after strengthening of *1.4 × the yield load* before strengthening. Also, the increase in the thickness of the concrete deck slabs was set at 8cm. According to the proposed design flow shown in Fig. 4, the various values are determined as shown in Fig. 5.

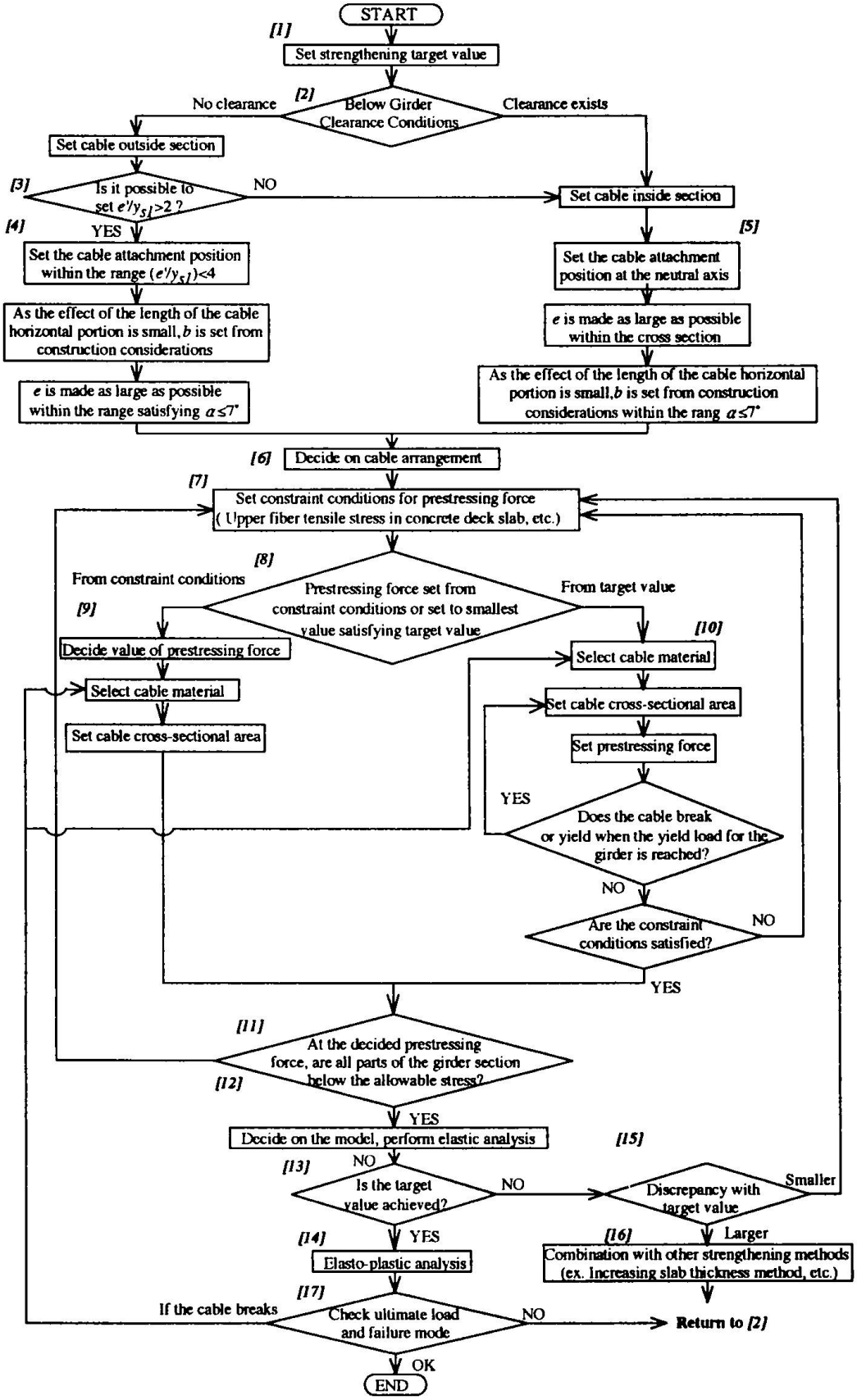

Fig. 4 Design procedure for strengthening existing bridges

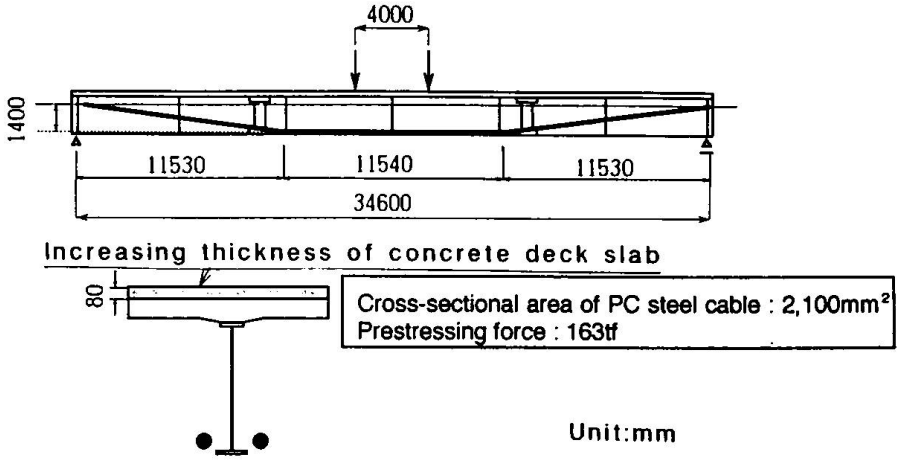

Fig. 5 Result of strengthening design by prestressing

The results of an incremental deformation method analysis performed with regard to the composite steel girder before and after the application of prestress, are shown in Table 2. From Table 2, it can be seen that the increase in yield load by a factor of 1.43 was achieved. With regard to other girder characteristics, the ultimate load was increased by a factor of 1.88, while the elastic range of the relation between the load and deflection at center span showed an improvement of 1.19 times for the gradient of the straight line portion of the curve.

Table 2 Analytical results of strengthening effect by prestressing

	Before strengthening	After strengthening (Steel strand)
Yield load (tf)	54.6	78.5 (1.44 times)
Ultimate load (tf)	96.7	181.9 (1.88 times)
Gradient of linear portion (tf/cm)	11.0	13.1 (1.19 times)

4. Conclusions

The main conclusions from this research can be summarized as follows.

1) From the experimental and analytical results, it was found that the prestressed composite girder has yield load and ultimate load superior to the standard girder, and that the performance is effected by the choice of cable arrangement and cable material.

2) With the objective of strengthening existing bridges, various dimensionless parameters were varied and an analysis made of the effects of these various parameters on the performance of the composite girder. Furthermore, a proposed design procedure based on the parameter analysis for the strengthening of existing bridges by introducing prestress to improve the yield load was successfully achieved and the efficiency of this strengthening method was adequately confirmed.

References

[1] Troitsky, M.S., "Prestressed Steel Bridges - Theory and Design," Van Nostrand Reinhold Company, New York, pp.1-16, 1990.

[2] Hoadley, G., "Behavior of Prestressed Composite Steel Beams," Jour. of Str. Eng., ASCE, Vol.89, No.ST3, pp.21-34, June 1963.

[3] Miyamoto, A., Hirata, K., Yagishita, F. and Mori, T., "Nonlinear Analysis of Prestressed Composite Girder and Its Application to Bridge Strengthening," Journal of Structural Engineering(JSCE), Vol.40A, pp.1101-1114, March 1994.

[4] Miyamoto, A., Yagishita, F., Maki, A. and Kobukata, Y., "Application of Prestressing Technique for Bridge Strengthening," Developments in Short and Medium Span Bridge Engineering '94, Nova Scotia, Canada, August 1994.

The Failure of Ancient Towers: Problems of their Safety Assessment

Luigia BINDA
Full Professor
Dept. Struct. Engineering
Milano, Italy

Anna ANZANI
Researcher
Dept. Struct. Engineering
Milano, Italy

Giulio MIRABELLA ROBERTI
Assistant Professor
Dept. Struct. Engineering
Milano, Italy

Summary

The safety of ancient towers has become a concern after some collapses which took place in recent years. Typical characteristic of most of these structures are not only the inhomogenity of the masonry itself but in many cases also the construction technique based on multiple-leaf walls, built in different phases with different materials. The survey carried out on the causes of the collapse of the Pavia Tower revealed a time-dependent behaviour of the material under heavy dead loads which was assumed to interpret the state of damage of a bell tower in Monza.

1. Introduction

Masonry is a composite material made with more or less regular layers of brick/stone and mortar. Its mechanical characteristics depend much more on the geometry of the components (shape, dimensions, thickness, etc.), on their mutual interaction, and on the way they are connected together, rather than on the mechanical properties of the components themselves.
In the past the global strength of the wall used to be increased by increasing the thickness of its section. Very often, for safety and economic reasons, building multiple leaf walls turned out to be more convenient. The way the leaves were connected together was depending on the shape and dimensions of the units, on the material used, on the construction technique which was different from site to site. Several times different materials were used in the leaves from regular stones and bricks to irregular stones, to concrete filling. The wall itself resulted a composite structure the response of which to dead and live loads is still badly known. For instance the application of modelling methods, like FE, or Discrete Element, is sometimes limited because suitable constitutive laws for these materials still have to be refined. Experimental results are still needed to understand the behaviour of these composite walls and learning from experience or even from failures can help to find the necessary information.
The results of two investigations will be briefly presented showing that the information collected after the failure of the Civic Tower of Pavia turned out to be useful for approaching the experimental study of the Bell Tower of the Cathedral of Monza.

2. Learning from a failure

On 17 March 1989 the Civic Tower of Pavia (Fig.1) suddenly collapsed killing four people. No apparent previous warnings were detected. Several hypotheses were formulated on the causes of the collapse, some of which were ruled out very soon. The construction took place in three to

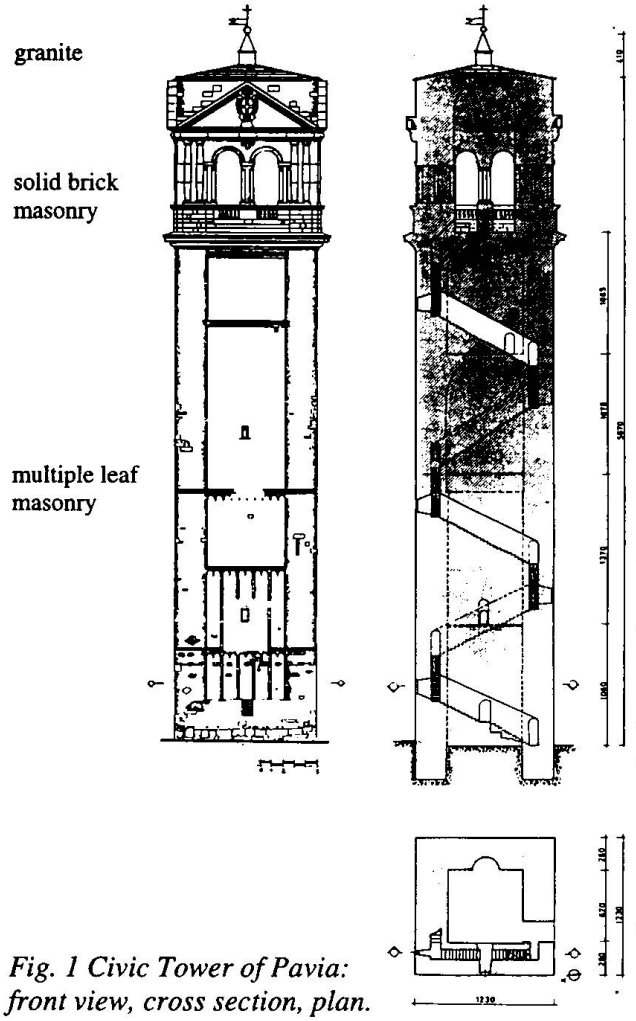

Fig. 1 Civic Tower of Pavia: front view, cross section, plan.

four phases, the first one between 1060 and 1100 AD, the second one between the XII and XIII century, while the belfry was added between 1583 and 1598.

For a thorough knowledge of the causes of the collapse an extensive experimental investigation was carried out on site and in the laboratory on the remainings of the tower. Approximately 100 large blocks of masonry were recovered for testing from the 7000 m^3 of ruins. The following procedure was adopted to determine the reasons of the collapse [Binda et al., 1992]:

- search of documents on the history of the Tower;
- reconstruction of the geometry of the Tower;
- geognostic tests to define consistency and mechanical properties of the soil;
- chemical, physical and mineralogical /petrographycal analyses of the mortars, bricks and stones;
- compressive tests on prisms;
- stress analysis of the Tower.

On the one hand settlements and chemical - physical damage were ruled out as causes of the collapse. On the other hand the following informations were found:

- the Tower was built in three to four different phases, using bricks and rubble materials until the belfry, which instead was built with granite blocks;
- a staircase built within the loadbearing wall ran along all the four sides of the Tower from the south-west corner up to the belfry;
- the total estimated weight of the Tower was 120,000 kN, while the weight of the belfry was 30,000 kN. The walls were multiple leaf walls with the external leaves were made with regular brick layers, the internal one was a sort of concrete made with layers of broken bricks and stones alternated with thick layers of mortar (Fig. 2);

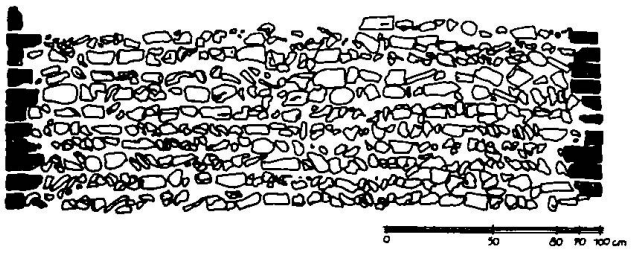

Fig. 2 - Cross section of the wall of the Civic Tower of Pavia

the lower part of the Tower was overstressed under its own weight. In fact maximum values of 1.7 to 2.0 N/mm^2 in compression were found by a FE elastic model, against experimental strength values ranging between 1.8 and 3.5 N/mm^2;

the material of the tower shown a time dependent behaviour under high stress level, which can bring the structure to collapse in a long time.

3. Behaviour of masonry walls as composite structures.

As mentioned above, the Tower of Pavia was made of multiple leaf walls, which is a typical technique frequently adopted in ancient buildings. The role of the leaves in load bearing walls is not always clear. It can range from the case of a main role of the external leaves, being the internal one a simple filling, to a load bearing role sheared among the three leaves, to the case of internal leaf which is the main one and the external ones play only the role of confinement or even framework. Moreover the leaves may be well connected horizontally with stiff long stones at given intervals or simply resting on continuous vertical mortar joints and when modelling the behaviour of this composite structure this should be taken into account [Binda et al. 1991, 1994].

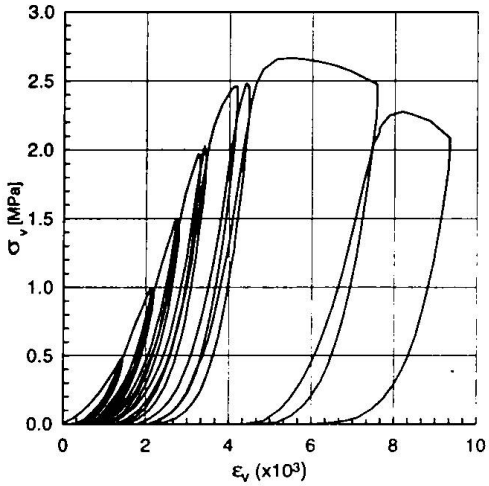

Fig 3 - Results of a test on a prism (400 x 600 x 700) mm^3 belonging to the masonry of the Civic Tower of Pavia.

In the case of the Pavia Tower the walls were continuous, more than 45 m high, 2800 mm thick, except where the staircase was running in a stairwell 800 mm wide. The thickness of external leaves was ranging between 150 and 450 mm only, that is 6 to 20% of the total thickness of the walls. They could have never supported a weight of 120000 kN without the collaboration of the internal leaf, which had actually to have played a loadbearing role.
In order to understand the mechanical behaviour of this masonry, mechanical tests had to be carried out on specimens representative of the inhomogeneity of the material of the internal leaf. Different kinds of compressive tests were carried out including tests applying unloading reloading cycles (fig. 3) and fatigue compression tests carried out to simulate the effects of the wind [Binda et al., 1992]. Creep tests were also carried out showing that these materials can be subject to an increasing damage when constant compressive stress is greater than the 50 to 60% of the peak stress; this damage can lead the material to failure when the stress value is higher than the 70% of the peak stress [Anzani et al. 1995].
Such a behaviour, the effects of which may be particularly heavy in the case of multiple leaf walls, is however typical also of the single components and of solid brick masonry. Therefore it has to be taken into account where the acting vertical stress is particularly high, as in the case of the dead load of ancient towers.

4. Experimental survey on the bell tower of Monza Cathedral

The bell Tower of the Monza Cathedral is a solid brick masonry structure dating from XVI century. This tower shows a considerable crack pattern which also in this case is probably due to the dead load, therefore many of the observations and hypothesis made in the case of Pavia Tower can be applied here, despite the different construction technique.
In order to investigate its behaviour experimentally, but having no possibility to sample a significant amount of material for testing, two wallettes have been cored, during the works for opening a door, from the crypt of the Duomo which has been built during the same period and reasonably likely with the same technique as the tower.
Prisms of about 200x200x500 mm have been obtained from the wallettes and have been subjected to three series of uniaxial compression tests of different type after being characterised

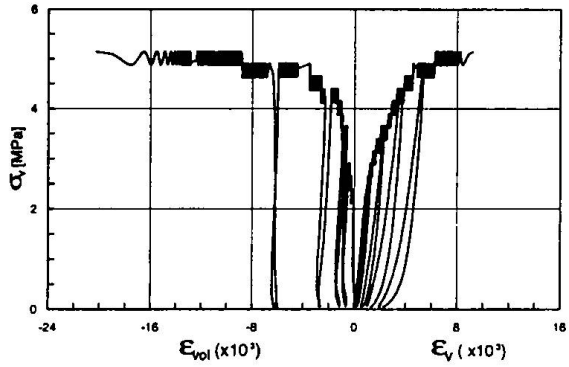

Fig. 4 - Results of a fatigue test carried out on a prism (200 x 200 x 500) mm³ belonging to the crypt of the Cathedral of Monza

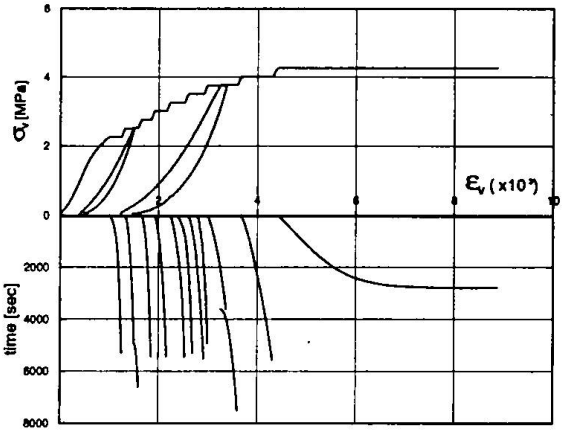

Fig. 5 - Results of a test with subsequent load steps carried out on a prism (200 x 200 x 500) mm³ belonging to the crypt of the Cathedral of Monza

through sonic tests: (i) monotonic tests have been carried out initially to have a first indication on the compressive strength of the masonry; (ii) cyclic tests were carried out subsequently during which cycles of ± 0.15 MPa at 1 Hz were applied at increasing stress levels; (iii) finally, compression tests were also carried out applying the loads in subsequent steps kept constant for a defined time interval of about 1.5 hours. Because any single test lasted more than one day, the samples were unloaded before night, for safety reasons, and reloaded the day after.

In fig. 4 the vertical stress vs. vertical and volumetric strain are shown, obtained with a cyclic test. It can be observed that during the application of the cycles a deformation takes place the amount of which becomes higher when the stress level is higher. Moreover, considering the volumetric strain, it appears that dilation occurs since the beginning of the test.

In fig. 5 the vertical stress vs. vertical strain and the vertical strain vs. time are shown, obtained with a test performed with subsequent load steps. Creep strain can be clearly observed during while load is kept constant, with the appearance of tertiary creep during the application of the last load step.

In fig. 6 the crack pattern at the end of the test of fig. 5 is shown, where vertical and diffused cracks can be seen indicating a severe damage of the material; this can also be detected if the increase in apparent volumetric strain and the apparent dilation of the material reported in the plot are examined.

Different in-situ tests have been performed to better understand the behaviour of the tower, like flat-jack test to measure the vertical stress and the stiffness of the material, together with an accurate geometrical survey and a description of the overall crack pattern.

In order to verify the response of the structure to dynamic loading and to verify the effect in terms of stress variation, two dynamic tests were planned using the environmental excitation: the first measured the

Lato C

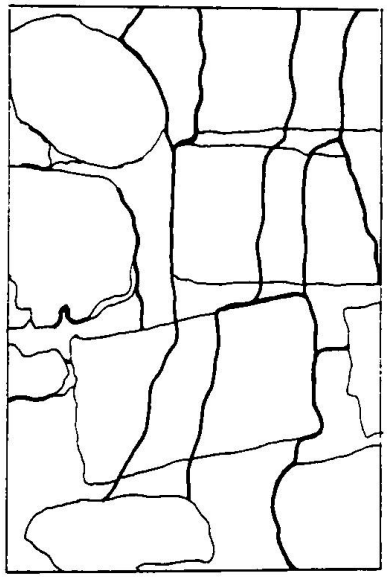

Fig. 6 - Crack pattern of the prism tested as reported in fig. 5.

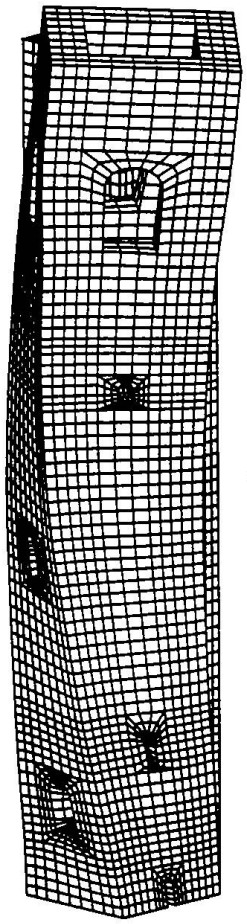

Fig. 7 - Modal form associated to the third frequency

effects of the bells ringing, the second one, not yet concluded, measured the effects of a strong wind. The response of six horizontal servo-accelerometers mounted in pairs at different height from the ground was monitored and elaborated, together with the readings of some transducers mounted across the major cracks near the front window at the base of the tower.

The sensitivity of the accelerometers is in the range of 0÷700 Hz, that is from the low (0.5÷5 Hz) frequencies expected for the tower movements to the frequencies associated with the sound propagation in the masonry.

By means of an appropriate analysis technique, acceleration histories are transformed in displacement histories at the different levels, giving a peak to peak maximum difference of nearly 4 mm in the W-E direction and of 1.9 mm in the N-S direction when all the bells ring together, and somewhat less (2.5 and 1.5 resp.) when only the major bell is ringing. In fig 7 the modal form associated to the third frequency of the tower is shown.

Also the transducers mounted across the major cracks are sensitive to the dynamic excitation induced by the bell ringing, giving a maximum peak to peak (opening to closing) of 28 μm, that should be compared with a daily variation of about 100μm due to temperature effects.

The analysis of the collected data allowed also to detect an important structural property, that is the frequency of the first mode of vibration of the tower. This value can be directly compared to the frequency obtained from a F.E. model of the structure, allowing to identify a dynamic elastic modulus that can be subsequently employed to calculate the effects (in terms of stresses) of the applied force history. For a more realistic approach, the modulus obtained in the unloading-reloading branches of the tests of fig. 4 was calculated, obtaining an average value of 3742±314 MPa.

The value adopted in the analysis was 3400 MPa, corresponding to a lower limit (but the specimen were cut from the crypt) and giving a very close match to the first frequency (0.654 Hz). Tab. 1 shows the frequencies calculated for the first 6 modes of the structure.

MODE	FREQUENCY [Hz]
1st flexural E-W	0.654
1st flexural N-S	0.663
torsional	3.178
2nd flexural E-W	3.232
2nd flexural N-S	3.311
axial	5.715

Tab. 1

A first dynamic analysis was made applying an harmonic force calculated from the movements of the mass of the main bell, in the form $F = F_h \sin(2\pi f t)$, with $F_h = 24.7$ kN and $f = 0.34$ Hz is the frequency of the bell oscillation. These calculations gave displacements very close to those measured experimentally, encouraging the use of the model for other verifications.

5. Conclusions

The investigation carried out after the collapse of the Pavia Tower allowed to understand the behaviour of the materials and the structures of the ancient towers.

Towers are generally subjected to heavy dead loads due to their height and their massive construction technique. As a consequence, the state of stress at ground level can be not so far

from the compressive limit strength of the material with the development of increasing creep deformation under constant loads. In the long run this behaviour induces a continuous damage of the material and can lead it to the collapse.
Similarly, the action of cycling loads can also increase very quickly the local deformations. The combined effect of these factors is able to induce severe conditions to the building, therefore when its structural stability is to be safeguarded any possible source of stress variation must be carefully taken into account including stress concentration due to geometrical discontinuity and the effect of wind action, bell ringing, daily and seasonal temperature variations.
If the structure is made with multiple leaf walls, a careful insight must be carried out to detect the thickness ratio between the leaves and the type of constraints which may or may not be present between them. In fact, the advantages given by the presence of the external leaves acting as a confinement can vanish if the connections are lacking or damaged.
Dynamic tests based on active excitation of the structure can inform about possible difference in stiffness along the height of the tower due also to material damage or to different construction techniques.

Acknowledgements
The research was supported by CNR-GNDT, MURST and by the parish of Monza.

References

ABRAMS, .D.P., NOLAND, J.L., ATKINSON, R.H, 1985, Response of clay-unit masonry to repeated compressive forces, pp 565-576, 7th IBMaC, Melbourne, Australia.

ANZANI, A., BINDA, L., MIRABELLA, G. , 1995, A Numerical Interpretation of Long-term Behaviour of Masonry Materials under Persistent Loads, pp. 179-186, 4th STREMA, vol. 1, Architectural Studies, Materials & Analysis, Computational Mechanics Publications.

BINDA L., FONTANA A., ANTI L. , 1991, Load transfer in multiple leaf masonry walls, 9th Int. Brick/Block Masonry Conf., Berlino, vol. 3, pp.1488-1497

BINDA, L., GATTI, G., MANGANO, G., POGGI,C., SACCHI LANDRIANI, G., 1992, The Collapse of the Civic Tower of Pavia: a Survey of the Materials and Structure, pp. 11-20, Masonry International.

BINDA L., FONTANA A., MIRABELLA G.,1994, Mechanical behaviour and stress distribution in multiple-leaf walls, 10th Int. Brick/Block Masonry Conf., Calgary, vol. 1, pp. 51-59

PAVESE, A. , 1992, Studi sul comportamento dinamico di torri in muratura e loro modellazione, PhD Thesis, Politecnico di Milano - University of Pavia.

RESENDE, L. , 1987, A damage mechanics constitutive theory for the inelastic behaviour of concrete, Computer method in applied mechenics and engineering, 60, 57-93.

Development of Composite Action in Existing Non-Composite Bridges

Ghislain DIONNE
Structural Engineer
Dessau inc.
Montreal, Canada

André PICARD
Professor
Université Laval
Quebec, Canada

Denis BEAULIEU
Professor
Université Laval
Quebec, Canada

Summary

An experimental investigation was undertaken to increase the load carrying capacity of existing slab-on-steel girder bridges without composite action. This particular type of bridge was mainly built 30 to 50 years ago. The main goal of this research was to provide a composite action between the concrete slab and the steel girders by means of fasteners. Many commercial anchors were tested and some prototypes as well. The results of this investigation are presented in this paper.

Introduction

Before the seventies, short and medium span steel bridges were frequently erected with a concrete deck directly cast on steel girders without any mechanical connection. Even if the theoretical evaluation of these bridges with actual truck loads shows underdesign conditions, the majority of these structures still behave relatively well. The main objective of the first part of the experimental investigation was to evaluate the carrying capacity of slab-on-steel girder bridges without composite action. Test results show that the flexural capacity of the steel beams is significantly increase because friction at the steel-concrete interface is sufficient to provide lateral restraint of the compression flange against lateral buckling (Dionne et al. 1994).

In this part of the experimental program, some specimens were strengthened with connectors to provide composite action between steel beams and concrete slab. Test results indicated that it is very important to eliminate the gap between the connectors and the surrounding materials. In fact, we found out that a relative displacement as small as 2 mm is sufficient to completely lose the composite action. Therefore, connectors should incorporate a device to fill the gaps in the holes of the beam flange.

In the second part of the experimental program, special connectors were designed and subjected to static and fatigue tests. Results of these tests are reported in this paper. The main objective of this research was to provide an efficient connection between the concrete slab and the steel girders by means of anchors.

Experimental program

The specimens used for the static and fatigue shear tests are shown in figure 1. A steel plate is connected to a reinforced concrete block with two anchors. The specified compressive strength of concrete was 30 MPa. The specimens were placed in a testing machine and the load was applied to the steel plate while the concrete block was held in place by a steel frame connected to the testing machine base.

Static shear tests were first carried out on various types of anchors in order to find out a shear connector which had a stiffness under service loads and an ultimate strength similar to end welded studs used in modern composite construction.

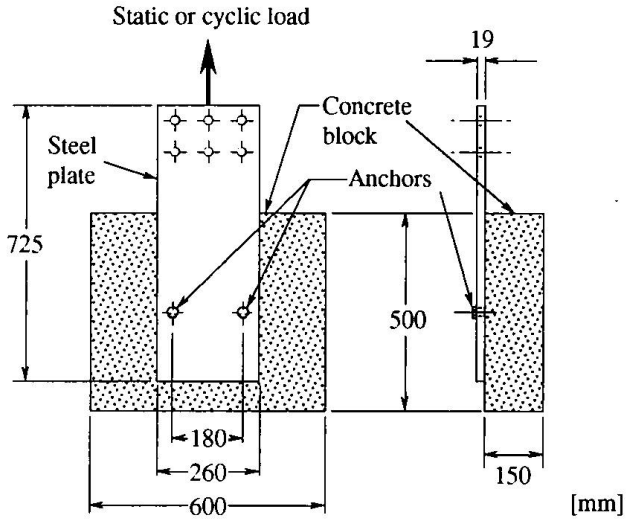

Fig. 1 Typical specimen used for shear tests

Many commercially available mechanical and chemical anchors were subjected to static shear tests. Mechanical anchors have an expansion device which presses against the wall of the hole in the concrete block while the anchor is tightened. Twenty one tests were carried out on seven different types of mechanical anchors. Chemical anchors comprise a threaded rod and a rapid setting epoxy which locks the anchor in the concrete hole. Eight tests were carried out on three different types of epoxy.

Commercial anchors are not designed with the requirement of eliminating the gap between the anchor rod and the hole in the steel plate (beam flange). The diameter of this hole is at least 2 mm larger than the diameter of the anchor rod to make the fastener installation easier. Although some anchors have an ultimate strength which compares well with end welded studs, slip under service loads is much higher and the composite action is impaired.

Therefore, some prototypes were designed to satisfy service load requirements, . The two most promising anchors are shown in Figure 2. The first one was obtained by adding a steel sleeve to a commercially available chemical anchors. Not only this sleeve eliminates the gap between the anchor rod and the plate hole but it also increases the shear strength at the steel-concrete interface, the most stressed cross section of the anchor rod. The second anchor (Fig. 2 b) has an inverted conical sleeve which expands and presses against the wall of the plate hole when the nut is tightened. The epoxy is injected into the concrete through a hole which is drilled along the longitudinal axis of the rod.

The anchors shown in Fig. 2 were specially designed to develop composite action in existing non composite bridges. Anchor installation on the bridge site is an important problem. There is no commercial machine which can perform the three main operations of the installation of an anchor, that is to drill a hole in the steel flange, in the concrete slab and to insert the anchor. Such an apparatus was devised and efficiently used to connect a concrete slab to steel girders (Croteau et al. 1996; patent pending). The apparatus includes a piston which firmly fix the machine between the beam flanges. It is indeed very important to immobilize completely the machine during the

three main operations of the installation of each anchor. The machine was designed to install mechano-chemical anchor with abutment sleeve (Fig. 2a) because it is the less expensive anchor.

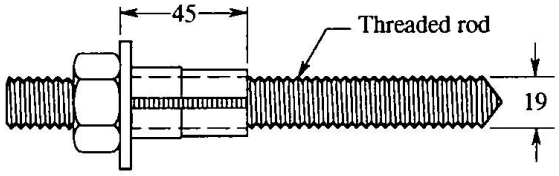

a) Mechano-chemical anchor with abutment sleeve

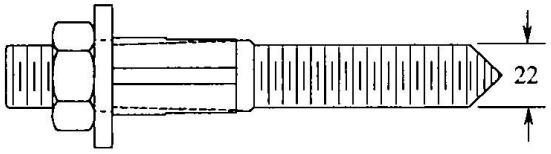

[mm]

b) Mechano-chemical anchor with inverted conical sleeve

Fig. 2 Mechano-chemical anchors

The anchors shown in Fig. 2, as well as shear studs, were subjected to cyclic shear loading at a stress range of 90 MPa (frequency : 10 Hz). According to the Canadian standard for bridge design (CSA 1988), shear studs should withstand 2 million cycles at this stress range. The maximum load of the loading cycles, which corresponds to the maximum service load, was determined from the following equation :

$$P_{max} = \frac{\bar{P}_u - 2s}{\gamma}$$

Where $\bar{P}_u$ is the average static ultimate shear load of the anchors (kN), s is the standard deviation (kN) and γ the safety factor ($\gamma = 3$). The minimum load of the loading cycles was computed to obtain a stress range of 90 MPa. For threaded rods, the shear stress is computed on the net area of the cross-section.

Test results

Tensile tests were carried out to determine the ultimate tensile stress (F_u) of steel used for studs and anchors. The average values of the measured ultimate tensile stress are as follows : 19 mm studs, F_u = 488 MPa; 22 mm studs, F_u = 499 MPa; anchors with abutment sleeve (Fig. 2a), F_u = 998 MPa; anchors with inverted conical sleeve (Fig. 2b), F_u = 579 MPa. Three tests were carried out in each case except for the 19 mm studs fir which six tests were carried out. The values of the coefficient of variation (standard deviation divided by the mean) are quite low (from 0.2% to 0.7%). High strength steel is used for threaded rods of anchors with abutment sleeve.

Static shear tests were first carried out to compare the behavior of commercial anchors to shear stud behavior. The stiffness under service loads is particularly important to maintain composite

action. Typical load-slip curves are shown in Figure 3. The initial portion of the curves which is enlarged, clearly shows that significant slip occurs at low load for both commercial anchors. As mentioned previously, tests on composite beams, where the slab was connected with commercially available anchors, have shown that the composite action is no longer effective when slip is larger than 2 mm. As shown in Figure 3, for commercial anchors, this critical slip is reached at low loads for commercial anchors compared to shear studs. It should be noted that the results shown in Figure 3 were obtained with the most efficient commercially available anchors.

Following these results, we tried to modify commercially available anchors and even designed some prototypes. The objective of this exercise was to come up with a connector as stiff as studs and offering similar ductility and ultimate resistance.

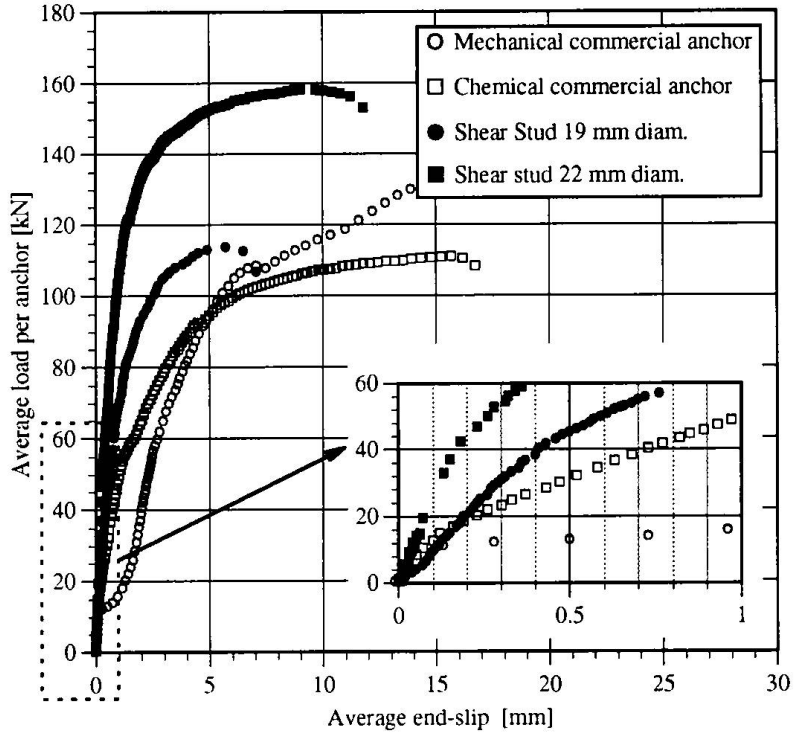

Fig. 3 Commercial anchors versus welded shear studs

The specially designed anchors shown in Figure 2 were first subjected to static shear loads in order to verify that stiffness under service loads and ultimate shear strength were similar to these of welded shear studs. As shown in Figure 4, the measured ultimate shear strength of mechano-chemical anchors with abutment sleeve is larger than the strength of 19 mm diameter studs but lower than the strength of 22 mm studs. The mechano-chemical anchors with inverted conical sleeve are as resistant as 22 mm diameter shear studs. Furthermore, we can see in the enlarged portion of the curves that both anchors have a stiffness under service loads clearly higher than the stiffness of 19 mm diameter studs. Therefore, both anchors justified further investigation.

In order to verify the behavior under cyclic loads, these anchors as well as studs were subjected to cyclic shear loading at a stress range of 90 MPa as explained previously. Two fatigue tests were carried out in each case except three tests for 19 mm studs. All anchors and studs sustained two million cycles of loading without fatigue fracture. The specimens were then statically tested up to ultimate load. Typical results are shown in Figure 5.

As we can see on this figure, the mechano-chemical anchors with abutment sleeve show less degradation under cyclic loads than the 19 mm diameter studs and even seem to have gained some

ultimate resistance. This increase is due to the orientation of the sleeve. We found out that when the slot is perpendicular to the direction of the shear force, the ultimate resistance increases by about 10%.

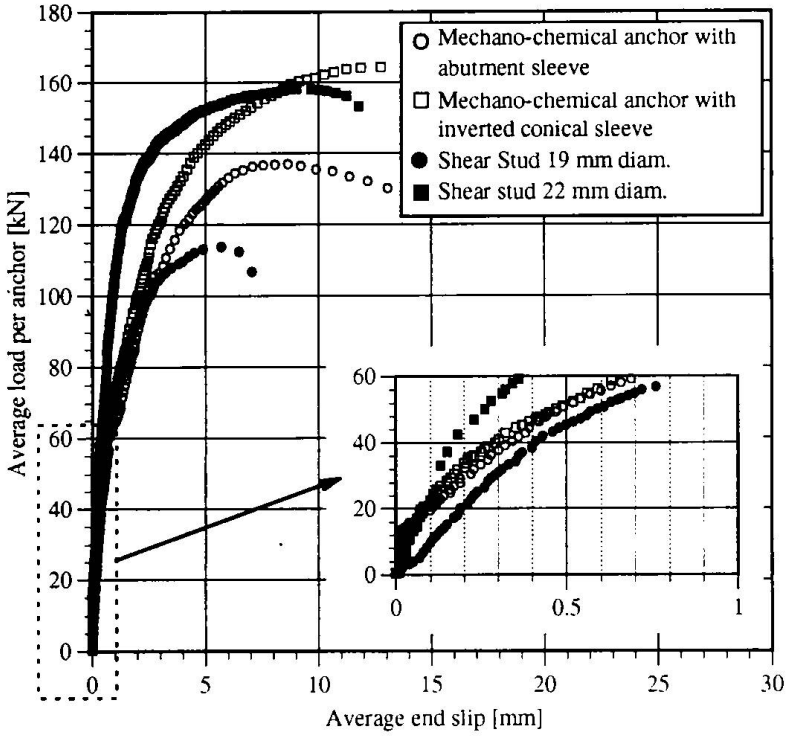

Fig. 4 Mechano-chemical anchors vs welded shear studs

By comparing the enlarged portions of Figures 4 and 5, it can be seen that there is no significant loss of stiffness in the service load range for both anchors after two million cycles, which is a suitable behaviour for bridge strengthening. It can also be seen that there is some degradation in the behaviour of welded studs since slip under service loads is larger for the specimens which were subjected to cyclic loading.

As shown in Figure 5, the behaviour of specially designed anchors is similar to the behaviour of 22 mm diameter studs. Even if the behaviour of both anchors is adequate, the anchor with an abutment sleeve is easier to fabricate and therefore cheaper. It was therefore recommended for further investigation (Croteau et al. 1996).

Conclusion

Commercially available anchors are not designed to efficiently strengthen slab-on-steel girder bridges. To be fully effective, the connector must be able to fill the space needed for its insertion. With this in mind, we designed prototypes in order to improve the stiffness of shear connectors at service load.

The two most effective prototypes developped to connect the concrete slab to steel beams were presented in this paper. They were devised to reduce as much as possible the relative displacement between the two materials. These anchors can develop full composite action and they well sustain cyclic loading. The strengthening technique can be used to connect the concrete slab to steel girders or transverse beams in existing non-composite bridges. The anchors can also

be used to improve composite action which has deteriorated due to slip increase at the steel concrete interface. This technique can also be used to upgrade the fatigue life of bridges who have reach a critical amount of sollicitation by adding additionnal connectors. Finally it is likely to consider the use of such anchors when the existing concrete slab or wood deck is replaced by a precast slab (Mohsen et al. 1995).

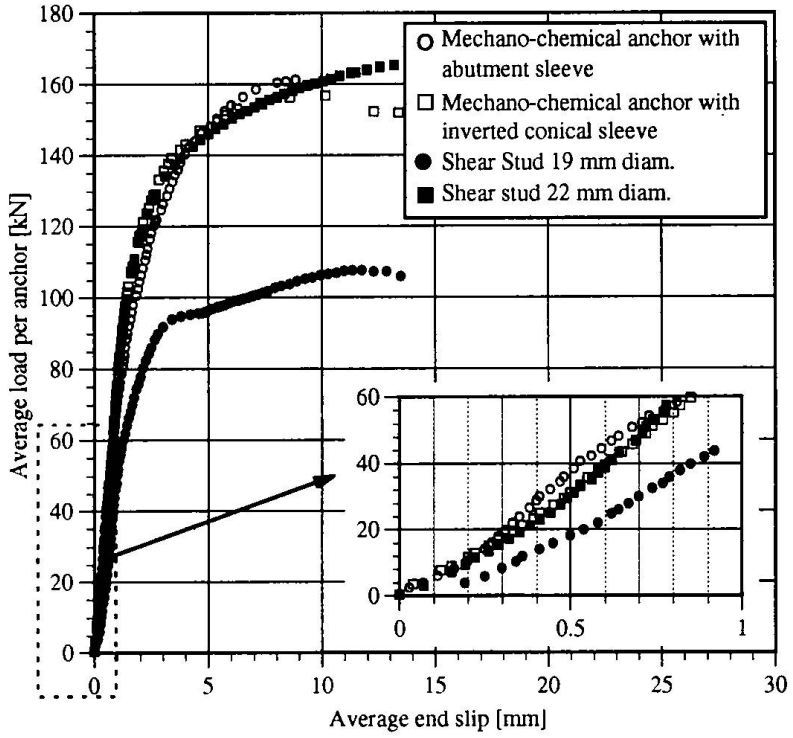

Fig. 5 Mechano-chemical anchors vs welded shear studs after 2 000 000 cycles

References

Canadian Standards Association, 1988. Design of highway bridges. Norm CAN/CSA-S6-88, Rexdale, Ontario, Canada.

Croteau, D., Picard, A., Beaulieu, D., 1996. "Renforcement des ponts acier-béton à l'aide d'ancrages mécano-chimiques, rapport GCI-96-12, Department of civil engineering, Laval University, 154 p.

Dionne, G., Beaulieu, D., Picard, A., 1994. "Évaluation expérimentale et renforcement des ponts en acier avec dalle de béton non participante". Canadian Journal of Civil Engineering, vol. 21, no. 2, pp. 329-339.

Dionne, G., 1996. "Comportement et renforcement des ponts acier-béton avec dalle non-participante", Ph. D. thesis, Department of civil engineering, Laval University, 367 p.

Mohsen, A. I., Alfred, A. Y., Mahmoud, A. I., 1995. "Construction procedures for rapid replacement of bridge decks". Concrete International, No. 1, pp. 49-52

Renewal of Bridge Superstructures under traffic at the A13 Brenner Motorway

Peter UNTERHOLZNER
Ingenieur
Alpen Strassen AG
Innsbruck, Austria

Peter Unterholzner, born 1940, received his civil engineering degree 1959 at the Technical College of Innsbruck.
Since 1973 chairman and since 1988 president of the Alpen Strassen AG.

Werner STIEBELLEHNER
Diplomingenieur
Wito-Konstruktionen Ges.m.b.H
Lienz, Austria

Werner Stiebellehner, born 1940, received his engineering degree 1966 at the Technical University of Vienna.
Since 1973 managing director of Wito-Konstruktionen Ges.m.b.H.

Summary

A number of bridge superstructures have been and will be repaired and renewed along the route of the A 13 Brenner Motorway in Tyrol, Austria. Hereby composites proved widely and advantageous. After a review on widening and repair work of various composite bridge decks it will be reported especially on the renewal of so-called 'Mushroom Bridge' deck slab by composite superstructures. The advantage of their construction, in particular, being accomplished under flowing traffic - even in winter - will be described.

1. Review:

In the course of widening works at the A 13 Brenner Motorway positive experiences were made with some composite bridges built more than 30 years ago.
A typical example was the widening of the two 'Gschnitztal Bridges' both situated side by side. There concrete deck slabs were dismantled and completely renewed one after the other. With the steel construction only the lower positioned windbracing had to be strengthened by welded straps. A number of aspects led to this success: higher concrete quality in connection with transverse prestressing (less weight), segmental concrete puring sections in artful sequence (higher grade of compound) and new calculation methods with meanwhile lowered prescriptions of traffic loads. Since both superstructures were widened one by one, traffic could flow during wintertime too. It was only restricted to one lane in each direction on one bridge. In the main travelling season both bridges were available, anyhow, with two lanes in each direction.

2. Disassembling and re-erection of so-called 'Mushroom Bridge' superstructures

These constructions are worth mentioning because of the very special solution and design work, which are required for the exchange of a superstructure carrying both traffic directions (full size bridge), without interruption of traffic.
It was an unavoidable condition that traffic could be restricted to one lane in each direction only between September and June. During the main season, however, two lanes in each direction have to be available.

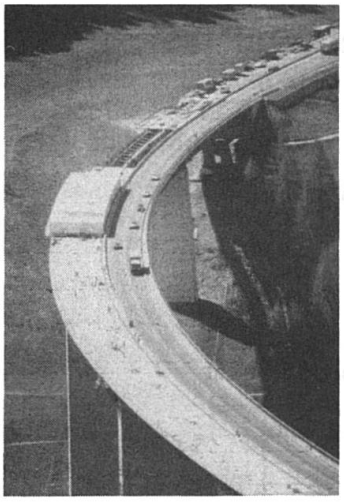

Fig. 1 Gschnitztal Bridges

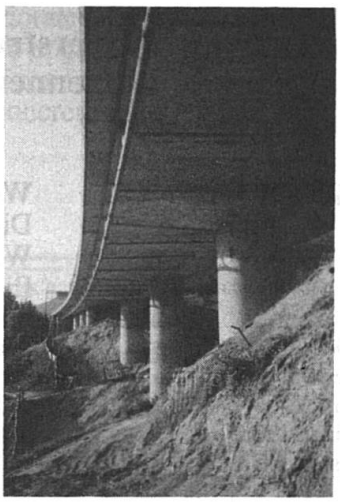

Fig. 2 Mushroom bridges (full size bridge)

2.1 The existing structures

The 'Mushroom Bridges' along the route of the A 13 were built thirty years ago. They are ten prestressed concrete bridges with a total area of 56.000 m². This variable bridge system was chosen at that time because of the difficult terrain situation, expected soil problems with the foundation as well as economic aspects. The full size bridges carrying both directions on one 'mushroom' have a typical span of 30 m. The half size bridges with only one traffic direction on a mushroom have one of 15 m. Each mushroom consists of a round, stiff bridge pier, which is fixed deap in the ground, and a very thin top slab being vouted towards the pier. Concrete hinges are connecting and supporting the mushroom structures.
During the time of existence, the influence of traffic loads and winter maintenance caused defects in all the system–required joints. Therefore an overall repair became necessary.
The repair work done at one mushroom bridge, by way of coupling together all the mushrooms to one single superstructure, proved almost as expensive as new bridge decks.

2.2 Project

An entirely new static system provides continuous beams supported by newly erected transverse pierheads which are attached to every old pier. This concept made it possible to support the superstructure as usual, but avoided a number of sensitive hinges and joints.
The first two bridges designed in this manner were put out for tender.The best bid was an alternative design which used composite instead of prestressed slab and beam construction. According to the good experiences with composites mentioned before, this variant design was applied by the authority to full and half size bridges.
Since the construction work under traffic is more remarkable in the case of full size bridges, this proceeding will be illustrated in detail.

2.3 Loads and design of composite superstructure

In addition to the standard loads, a 100 ton heavy vehicle load was taken into account with the static calculations. The final system of a full size bridge is a continuous superstructure of 1,8 m height. It consists of six steel main girders in longitudinal direction, a transverse steel truss every 6 m and a concrete deck slab, which is typical 22 cm thick.

2.4 Construction

Boundary conditions caused by the influence of traffic led to the following construction sequence within 3 working seasons – allways from September to June

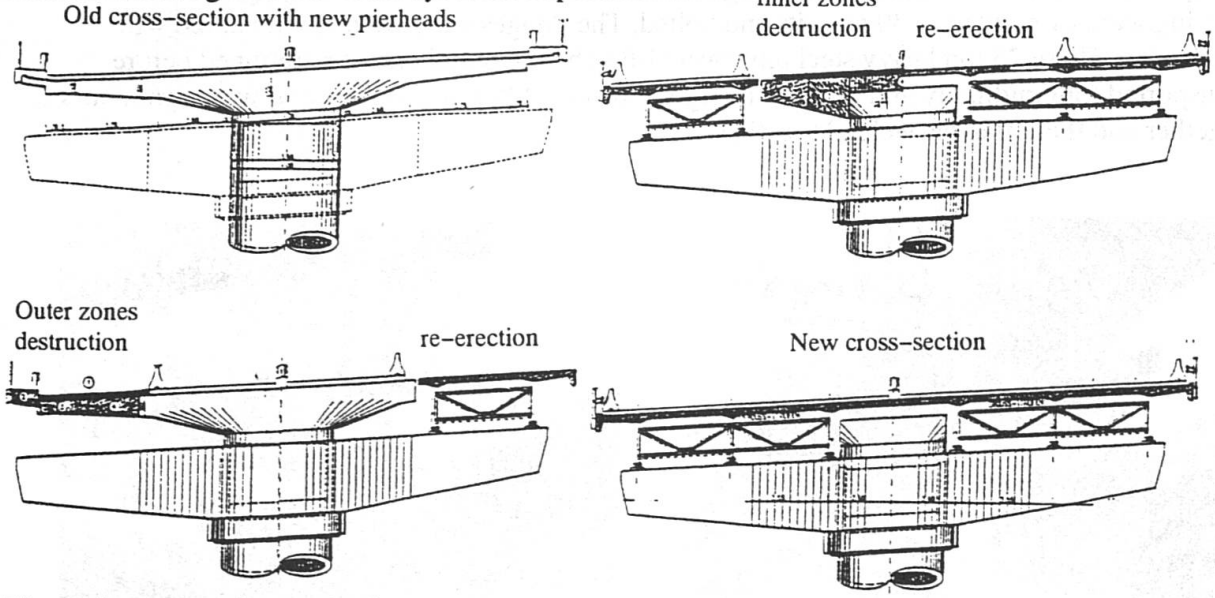

Fig. 3 Sequence of construction

From October 1992 to June 1993 the first half size mushroom bridge decks were reconstructed and new transverse pierheads for the full size bridge installed. In fall, winter and spring of 1993/94 the outer deck slab region and within the same period in 1994/95 the inner deck slab region were dismantled and re-erected. Two traffic lanes were always available, first at the inner and then at the new auter region. During each summer, traffic was flowing on both parts using four lanes. Speed was reduced to 80 km/h.

2.4.1 Destruction

The destruction of the bridge deck from out- to inside was exactly prepared. The concrete was machine cut by large diamond saw blades or in case of bigger volume by rope saws. For transportation two portal cranes were used being moved on longitudinally situated rails. The shipping weight of the concrete blocks lay between 6 and 18 tons.

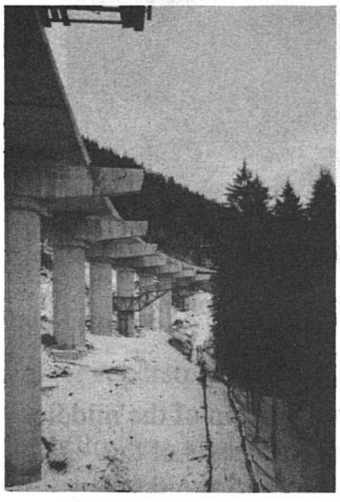

Fig. 4 Destruction outer deck slab

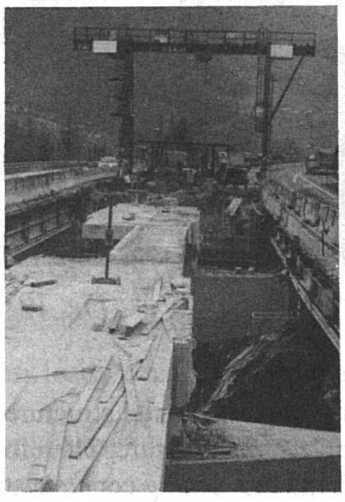

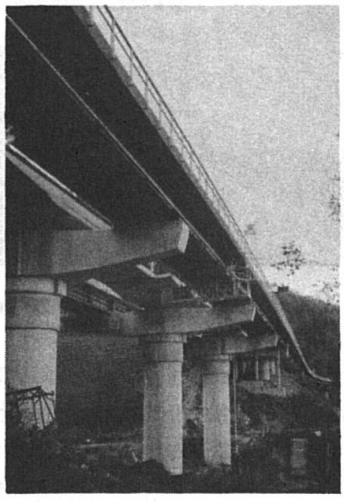

Fig. 5 and 6 Destruction inner deck slab

2.4.2 Steel Construction

The steel structure was produced in factory, derusted by sandblasting and coated with the first layer or with a rub resistant coating in the region of friction–type connections. Out side the actual bridge area (before or behind) four main girders, the transverse trusses belonging to them and the bracing were assembled in 30 m units and bolted. The flanges were welded with cored wire electrodes. These 23 ton heavy steel units were lifted by the portal cranes mentioned before, transported longitudinally and set into the right position. After that unit by unit were again bolted together and there flanges welded together.

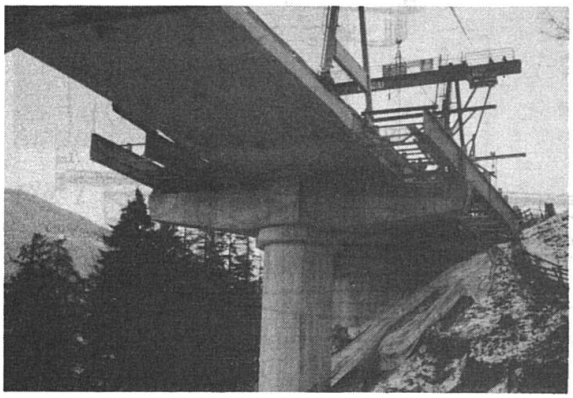

Fig. 7 Setting of steel units at outer structure

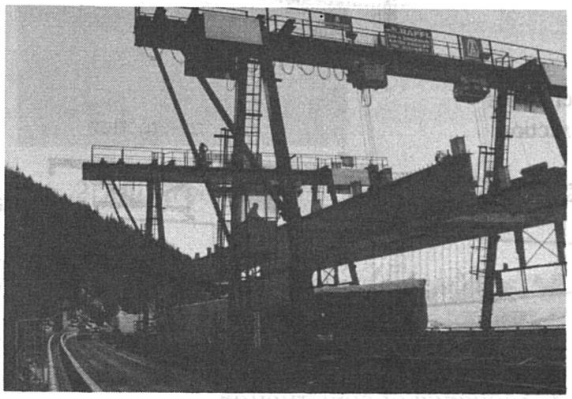

Fig. 8 Setting of steel units at inner structure

The assembling work and job site welding were done in wintertime, from December until March.

2.4.3 Top slab

The concreting of the top slab was done in 15 m units within five days. Gaps were left between in order to reduce the tensile stresses. Form carriages were moved on rails installed above and supported by lost concrete pads. By encasing and heating the form carriages, a continuous working cycle was possible even in wintertime.

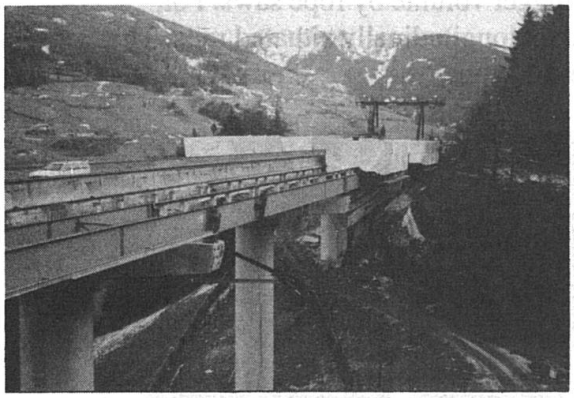

Fig. 9 Concreting at outer structure

Fig. 10 Concreting at inner structure

2.4.4 Completion

In the last construction phase the completed outer structure and the raw construction of the middle structure were unified to one single superstructure. Therefore the remaining steel parts of the transverse trusses were installed and the closing concrete stripes casted. In order to avoid strong vibrations this was done on the weekends when no trucks were going.

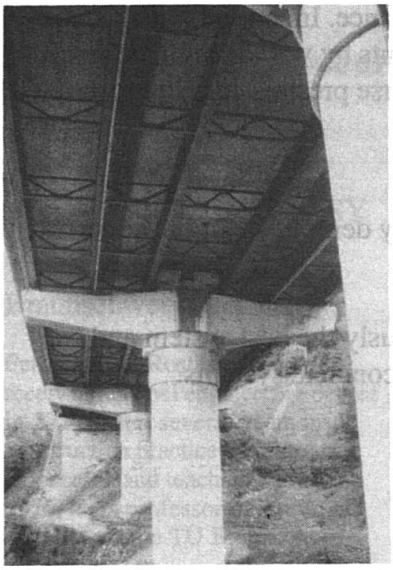

Fig. 11 Completed bridge

Both bridges were completed in time.

3. Preview

Because of its success the described method of renewing the bridges described before was also applied to further objects. 3 bridges are in reconstruction at the moment. They are expected to be completed by the summer of 1998.

4. Conclusion

Only because of the advantages of composites, the short schedules could be met, despite the narrow space situation beside traffic and the seasonal weather conditions.

The following advantages of the composite construction system were essential:

Labour and supervision intensive work on site are reduced by a far–reaching preproduction of the steel structure in the workshop and simple assembling on site.

Composite construction is a simple system which manages without heavy and costly scaffolding.

Overlapping steel and concrete work is possible by way of concreting the top slabs in segments one by one.

Continuous construction without delay can be done even in winter. Steel erection and welding with cored wire electrodes too is possible without any problem at minus degrees.

Only concreting in segments allows encasement and heating.

Lighter superstructures are possible with less load on piers and foundation.

The following advantages of composites will be useful in the future:

The composite deck is a wearing part with less lifetime than the rest of the structure. It can be removed and renewed in a simple way.

Composites can be changed easily, strengthened and widened for instance. Increased traffic loads and/or wider decks can be achieved in accordance to static requirements by way of higher rate of compound, higher concrete quality and reinforcement ratio or transverse prestressing. In most cases the steel part can be strengthened slightly and easily.

Maintenance is less expensive than with solid concrete structures.

And last but not least: in case of a pulling down of the bridge, the easy demolition of the concrete part and the easy recycling of the steel part are worth mentioning.

In view of economy and ecology the composite construction is obviously the best system and can compete – especially under certain circumstances – with prestressed concrete systems.

Involved Parties

Owner:
Austrian Federal Ministry for Economic Affairs
Bundesstrassenverwaltung Abt.VI/7
Stubenring 1
A-1011 Wien

Alpen Strassen AG
A-6020 Innsbruck, Austria

Design:
Tender project, design substructure and dismantling sequence
Kirsch – Muchitsch and partners, Consulting Engineers
Linz, Austria

Composite superstructure
Baumann – Obholzer, Consulting Engineers
Innsbruck, Austria

Supervising engineer:
Prof.Dipl.-Ing.Dr.techn.Manfred Wicke
Innsbruck, Austria

Contractor:
Concrete Joint Venture 'Mayreder-Innerebner-Stuag'
Steel Joint Venture 'Raffl-Wito-Hamberger'

References:

(1) Tschemmernegg F., Passer H., Neuner O.,Sporschill K.:
Verbreiterung und Sanierung von Stahlverbundbrücken
Stahlbau 60 (1991), Heft 10 S. 289.298

(2) Tschemmernegg F.: Schnelle wartungsfreundliche Brückenlösungen durch Stahl.
Vortrag zum Symposium 'Stahl u. Stahlbau' Innsbruck 1992

(3) Obholzer A., Brandstätter H.: Sanierung Reichenbichlbrücke und Kl. Larchwiesenbrücke,
Lösung mit Stahlverbundvariante. Stahlbau-Rundschau 83/1994, S 25 - 27.

(4) Stiebellehner W.: Neue Stahl-Verbund-Strassenbrücken
Vortrag zum Österreichischen Stahlbautag 1995

(5) Wicke M., Kirsch P.: Abtrag und Tragwerkserneuerung bei Pilzbrücken der
Brenner Autobahn unter Verkehr. Bauingenieur 71 (1996), H. 4 S. 145-153.

(6) Unterholzner P., Obholzer A.: Erneuerung von Brückenbauwerken unter Verkehr
auf der Brenner Autobahn A13. Stahlbau 65 (1996), Heft 7 S.233-239